1999

Influence of pre-existing corrosion pits on fatigue life in a 2024-T3 aluminum alloy

Baekho Lee
Lehigh University

Lee, Baekho

Influence of pre-existing corrosion pits on fatigue life in a 2024-T3 aluminum alloy

May 31, 1999

INFLUENCE OF PRE-EXISTING CORROSION PITS ON FATIGUE LIFE IN A 2024-T3 ALUMINUM ALLOY

by

Baekho Lee

A Thesis

Presented to the Graduate and Research and Committee

of Lehigh University

in Candidacy for the Degree of

Master of Science

in

Mechanical Engineering

Lehigh University

April, 1999

This thesis is accepted and approved in partial fulfillment of the requirements for the Master of Science.

April 27, 1999

Date

Dr. Robert P. Wei
Thesis Advisor

Dr. Charles R. Smith
Chairperson of Department

ACKNOWLEDGEMENT

I would like to express sincere appreciation to my advisor, Professor Robert P. Wei, for his invaluable guidance and support throughout this thesis. Without his patience, encouragement, and technical background, this work could not be done in an appropriate time. I also wish to acknowledge my undergraduate advisor Dr. Rer Nat Jai-Sung Lee for providing me with the opportunity to pursue the oversea study. Much thanks also go to Mr. Evan J. Dolley for his endeavor teaching me how to do things during this thesis.

I wish to thank Lehigh University for the tuition support during a portion of my study. The kindness from Mrs. Shirley Simmons, technical assistance from Messrs. Carl D. Miller and friendship from Dr. Chi-Min Liao, Evan J Dolley, Carl H. Iwashita, Svetlana P. Oshkai, Pål Ove Pederson, and Zhifan Huang are truly appreciated. I also acknowledge Julie DeMoyer for her previous research on 2024-T3 central circular hole specimen.

Finally, I am grateful to our parents, brothers, and sisters for their consistent encouragement. I sincerely dedicate this thesis to my wife, Wonhee. Her understanding, patience, and sacrifice during these years with our first baby, Jenny, will be in my heart, forever.

TABLE OF CONTENTS

LIST OF TABLES

LIST OF FIGURES

ABSTRACT

The primary objectives of this work are as follows: (1) to experimentally examine the influence of pre-existing corrosion pits on fatigue life and (2) to determine if fatigue life can be predicted from initial pit sizes and known fatigue crack growth (FCG) properties. This work explores the feasibility for establishing a framework for the prediction of fatigue life in a corrosive environment.

Experiments were conducted on single-edge-notch (SEN) specimens of a 2024-T3 aluminum alloy. The notch surface on the specimens was pre-corroded in 0.5M NaCl solution (pH $\approx$ 6.5, $[O_2] \approx 7$ ppm) from 48 to 384 hours (2 to 16 days) at room temperature (~ 20°C). Uni-axial fatigue experiments were performed at room temperature under a stress range of 288 MPa at the notch root with a load ratio of 0.1 and frequency of 30 Hz. The fatigue fracture surfaces were examined by scanning electron microscopy (SEM) to identify the crack nucleation sites and to determine the size and geometry of nucleating pits.

Pre-corrosion was found to reduce the subsequent fatigue life of notched specimens. The reduction was by more than one order of magnitude after 384 hours of pre-corrosion relative to the lives of the uncorroded specimens, and is correlated with the size of the nucleating corrosion pits, ranging from 15 to 60 μm. This finding is consistent with the result of an earlier study on smooth specimens of 2024-T4 aluminum alloy tested in rotating bending.

Fatigue lives were estimated on the basis of fatigue crack growth from a dominant corrosion pit using linear elastic fracture mechanics. The estimated fatigue lives were

found to be in good agreement with the observed fatigue lives. By inference, the process for fatigue crack nucleation from a corrosion pit was brief, and its contribution to fatigue life may be neglected. Based on the measured distribution in pit sizes, the distribution in fatigue lives following a given period of pre-corrosion were estimated, and was found to be in good agreement with experimental observations.

Taken together, these results showed that accurate predictions of fatigue lives can be made based on information on the pitting and fatigue crack growth properties of the material alone.

CHAPTER 1 INTRODUCTION

1.1 MOTIVATION OF THE STUDY

Commercial and military aircraft are typically constructed of 2XXX and 7XXX series aluminum alloys because of their attractive engineering properties such as high strength/weight ratio, good fracture toughness, and low cost. Many of the aircraft were originally designed for a service objective of 20 years but because of economic considerations these airplanes are remaining in service beyond that service objective. As the airplane ages, the effect of corrosion becomes more pronounced. The coupled effect of corrosion with fatigue cracking is the most important structural problem of aging aircraft. Corrosion is a form of material damage caused by the exposure of metals to corrosive environments such as moisture, acid rain, and other electrolytes. One typical form of localized corrosion in aluminum alloys is pitting. Because corrosion pits can act as nuclei for fatigue cracks in the structure, it is of major concern in the maintenance of structural durability and integrity. The Aloha incident in 1988 [1,2] is a well-known example of the effect of corrosion on the structural integrity and safety of aircraft. Identification of pitting and quantification of its impact on fatigue life for a high-strength 2024-T3 aluminum alloy have been done by several researchers [3-9]. The effect of pitting damage on subsequent fatigue life has been experimentally studied [10,11]. Corrosion pits were believed to be nuclei for fatigue cracking in aircraft structures [12,13,14].

Although some studies have demonstrated that reductions in fatigue lives are associated with corrosion pits, little systematic analysis has been made with the aim of

developing a quantitative method for prediction. The role of pre-existing corrosion pits on fatigue life in a 2024-T3 aluminum alloy has been studied recently at Lehigh University [12,15]. Many issues, however, remain to be solved.

1.2 Statement of Thesis

The effect of pre-corrosion on the fatigue life of a high-strength 2024-T3 aluminum alloy subjected to a constant amplitude loading condition has been investigated [11]. Pitting corrosion is believed to be a typical degradation mechanism for damage in aqueous environments. Pits as nuclei for fatigue cracking have been investigated, and it is known that they supplanted the early growth (nucleation) portion of the fatigue life. The objective of this study is to determine the effect of pit size on fatigue life and if fatigue life could be estimated as a function of the nucleating pit size and known fatigue crack growth (FCG) properties. To meet this objective, it is necessary to experimentally characterize the effect of initial pre-corrosion pit of different sizes on fatigue behavior, to correlate the pit sizes to the actual fatigue life, and to estimate the fatigue life based on the FCG rates. Based on this work, the feasibility of establishing a framework for engineering methodology for predicting the fatigue lives of pre-corroded 2024-T3 aluminum alloy is considered.

1.3 Structure of Thesis

Chapter 1 is an introduction that describes the motivation, fundamental issues, and objectives for this thesis.

Chapter 2 is a review of the technical background that contains conceptual bases and previous studies relative to the current research.

Chapter 3 is a description of the experimental settings and approach, which include specimen design and preparation, experimental apparatus, procedure and observation.

Chapter 4 is a description of the experimental results. Test results on fatigue experiment based on fractographic observation are described. For comparison with this study, the results from a previous research by Harmsworth are summarized.

Chapter 5 is a discussion of the estimated fatigue lives as compared to the actual fatigue lives. Estimation of fatigue life for crack growth was made either by simple integration of a power-law relationship or by using a computer program for fatigue analysis, AFGROW.

Chapter 6 is the summary and conclusions of this research followed by suggestions for future work.

CHAPTER 2 TECHNICAL BACKGROUND

2.1 INTRODUCTION

This chapter describes the current state of understanding for fatigue cracking coupled with pitting corrosion. Definitions and determinations of pitting corrosion are first reviewed. Fatigue in the design for durability and integrity of structures subjected to cyclic loading (for example, that associated with fuselage pressurization and depressurization) is reviewed, with special emphasis on fatigue crack growth (FCG) and previous researches in this area. Figure 2.1 shows a schematic diagram of the development of corrosion fatigue. The early stage is dominated by corrosion, in the form of pitting corrosion and the later stage by corrosion fatigue crack growth. Figure 2.2 shows a typical corrosion fatigue cracking which was nucleated at a corrosion pit.

2.2 PITTING CORROSION

One form of localized corrosion is pitting which can lead to the nucleation of fatigue cracking. This process of pitting and fatigue cracking is considered as a principal degradation mechanism [8,12,13]. Pitting can significantly reduce or eliminate the initial (or nucleation) portion of the fatigue life and compromise structural durability and integrity. Because of its widespread occurrence and damaging effect, pitting has been a matter of concern in many industrial applications for several decades. Extensive studies of a 2024-T3 aluminum alloy have been undertaken to determine conditions that cause pitting and to understand the basic processes involved [5,8,12,13].

Referring to this study, the microstructural investigations show a typical elongated and flattened grain structure, with average grain dimensions of 68 μm, 39 μm and 18 μm in the longitudinal (L), transverse (T), and short transverse (S) direction, respectively shown in Figure 2.3 [5]. Extensive experimental data have been gathered and a major progress has been made in both the understandings of the principal causes of pitting initiation and growth. The current state of understanding is briefly summarized. Many important issues, however, remain unresolved.

2.2.1 PITTING

Pitting is one of eight forms of corrosion. It is one form of extremely localized attack, and is destructive and insidious. Basically, it is the process of electrochemical reaction of galvanic coupling between two different metals in aqueous environments. Alloys are characteristically inhomogeneous. If a particle or particle clusters are exposed to the corrosive environment, galvanic coupling between particle and matrix would promote either anodic dissolution of the matrix around the particle or dissolution of the particles. Representative SEM micrographs of the same area of an aluminum alloy before and after corrosion in 0.5M NaCl solution for 24 hours are shown in Figure 2.4 [9]. As the corrosion time increases, the matrix around particles dissolves generally or severely based on the size of the particles or particle clusters in Figure 2.5 [9]. These severe pits can act as nuclei of fatigue cracking based on its size and location.

2.3 FATIGUE

Fatigue cracking in the presence of corrosion has long been considered as a principal degradation mechanism for material damage in service. The influence of pitting corrosion on fatigue life was recognized through the works of Haigh [16], Moore [17], and Gough and Sopwith [18] early this century. Separate from the S-N approach, a methodology based on linear elastic fracture mechanics (LEFM) was introduced by Paris and Erdogan [19] using a power-law representation of the relationship between crack growth rate and the driving force. The power-law relationship is essentially empirical, however, cannot explicitly account for the influence of environment. Critical reviews and analysis of empirical and statistical approaches were given by Wei [20].

Corrosion fatigue crack growth in corrosive environment has been extensively studied [3,21-26] to develop a mechanistic understanding of the influences of mechanical, environmental, metallurgical, and geometrical variables. The many variables are summarized in Table 2.1 [20] and serve to emphasize the complexity of corrosion-fatigue behavior. Currently, empirically based power-law models are used in life prediction methodologies. Ideally, it is desirable to characterize the corrosion fatigue of a material to represent the fatigue life, N_f, or the fatigue crack growth rate (FCGR), da/dN, as a function of these variables; i.e.,

$$N_f = F_1 (\sigma_{max}, R, f, T, p_i, C_i, \cdots) \tag{2.1}$$

$$da/dN = F_2 (K_{max}, \text{ or } \Delta K, R, f, T, p_i, C_i, \cdots) \tag{2.2}$$

2.3.1 Mechanical Driving Force for Fatigue Crack Growth

The stress intensity factor, K, characterizes the magnitude of the stresses in the vicinity of the crack tip. It is a function of crack length, applied stress, and geometry. For cyclic loading, the stress intensity factor range, ΔK (K_{max} – K_{min}), is used to characterize the mechanical driving force of FCG to provide correlation with the FCGR, da/dN [20]. It is used principally for crack opening mode conditions, Mode I (tension), when the assumptions of linear elastic fracture mechanics (LEFM) are satisfied. For other loading conditions, such as Mode II (sliding) and III (tearing) and mixed-mode loading, the use of strain density factor range, ΔS, has been suggested [27].

2.3.2 Fatigue Crack Growth Rate

Due to the application of a number of cycles ΔN, the crack length increases by an amount of Δa. This rate of growth is typically calculated by dividing the growth increment by the number of elapsed cycles as $\Delta a/\Delta N$. For small intervals, this average (or "*secant*") rate is taken to be approximately equal to the FCGR. The growth rate is a function of the loading, environmental and material variables and may be determined by numerical differentiation of the set of crack length versus cycles (a vs. N) data.

$$\frac{da}{dN} \approx \frac{\Delta a}{\Delta N} = F\left(K_{max}, \text{or } \Delta K, R, f, T, p_i, C_i, \cdots\right) \tag{2.3}$$

For given material and environmental conditions, the fatigue growth response is commonly represented by an empirical relationship between da/dN and ΔK of the following form, where C is the growth rate coefficient and m is an exponent.

$$\frac{da}{dN} = C(\Delta K)^m \tag{2.4}$$

The experimental results may be plotted in log(ΔK)-log(da/dN) diagram to determine the constant C and slope m. Once the quantities are determined, the fatigue life, N_f, can be estimated by direct integration between the initial and final crack sizes, based on information on geometry and loading conditions.

2.3.3 Transition from Pitting to Fatigue Cracking

For engineering materials, fatigue cracking in an inert environment typically nucleates for inhomogeneities in the microstructure (e.g., large constituent particles) or other sites of stress concentration. In corrosive environment, crack can begin at sites of localized corrosion damage, such as corrosion pits. Once nucleated the crack progresses as a surface crack, and transitions to a through-thickness crack, and can lead to fatigue failure. The process of crack nucleation (or the transition from pitting to surface crack) is important to the estimation of corrosion fatigue life [28,29]. The following criteria have been proposed for the transition from pitting to FCG, i.e., the onset of fatigue cracking from a corrosion pit [30,31],

$$\Delta K \geq \Delta K_{th} \tag{2.5}$$

$$\left(\frac{da}{dt}\right)_{crack} \geq \left(\frac{da}{dt}\right)_{pit} \tag{2.6}$$

where (da/dt) refers to the appropriate crack and pit growth rates, and ΔK_{th} is the threshold ΔK for fatigue crack growth; ΔK is estimated by assuming that the corrosion pit may be modeled by an equivalent semi-elliptical (or semi-circular) surface crack.

Specifically, fatigue cracking would occur only when the stress intensity factor ΔK of the equivalent crack reaches or exceeds the threshold ΔK_{th}, and when the time based crack growth rate exceeds the rate for pit growth. The criteria have been verified experimentally [13,32] and statistically [15]. For the pre-corroded specimens used in this study, only the threshold criterion would apply.

2.3.4 Estimation of Fatigue Life

As described in section 2.3.2, the fatigue lives of specimens or components with simple geometry and loading conditions can be estimated by direct integration of the growth rate Eq. (2.4) if the initial crack size is given. Such a procedure was used to estimate the effect of corrosion (pitting) on fatigue lives of an aluminum alloy [33].

Assuming that the initiating defect is hemispherical in shape and is equivalent to a semi-circular crack with the same aspect ratio, the power-law relationship has been used to construct S-N curves shown in Figure 2.6 [33]. These curves indicate the severe reduction in fatigue life as the size of the initial corrosion pits increases, or as the frequency decreases thereby increasing the corrosion time per loading cycle.

For more complex geometries and loading conditions, numerical integration is required, using one of the specialized computational programs. AFGROW [34] is one such computer software that is developed for fatigue crack growth analysis and life prediction. This program can handle different specimen geometries, component and crack as well as constant and variable amplitude loading. It is adopted for use in this research.

Table 2.1 Significant variables that influence the corrosion fatigue [22].

- *Mechanical Variables*
  - ◊ Maximum stress or stress intensity range, σ_{max} or K_{max} [1]
  - ◊ Cyclic stress or stress intensity range, $\Delta\sigma$ or ΔK [1]
  - ◊ Stress ratio, or load ratio, R [1]
  - ◊ Cyclic load frequency, f
  - ◊ Cyclic load wave-form (constant amplitude loading)
  - ◊ Load interactions in variable amplitude loading
  - ◊ State of stress
  - ◊ Residual stress

- *Geometrical variables*
  - ◊ Crack size and relation to component dimensions
  - ◊ Crack geometry
  - ◊ Component geometry adjoining crack
  - ◊ Stress concentrations associated with design

- *Metallurgical Variables*
  - ◊ Alloy composition
  - ◊ Distribution of alloying elements and impurities
  - ◊ Microstructure and crystal structure
  - ◊ Heat treatment
  - ◊ Mechanical working
  - ◊ Preferred orientation of grains and grain boundaries (texture)
  - ◊ Mechanical properties (strength, fracture toughness, etc.)

- *Environmental variables*
  - ◊ Temperature, T
  - ◊ Types of environments – gaseous, liquid, liquid metal, etc.
  - ◊ Partial pressure of damaging species in gaseous environment, p_i
  - ◊ Concentration of damaging species in aqueous or other liquid environment, C_i
  - ◊ Electrical potential, ϕ
  - ◊ pH
  - ◊ Viscosity of the environment, η
  - ◊ Coatings, inhibitors, etc.

[1] These three parameters are inter-related. Only two of the three need to be specified.

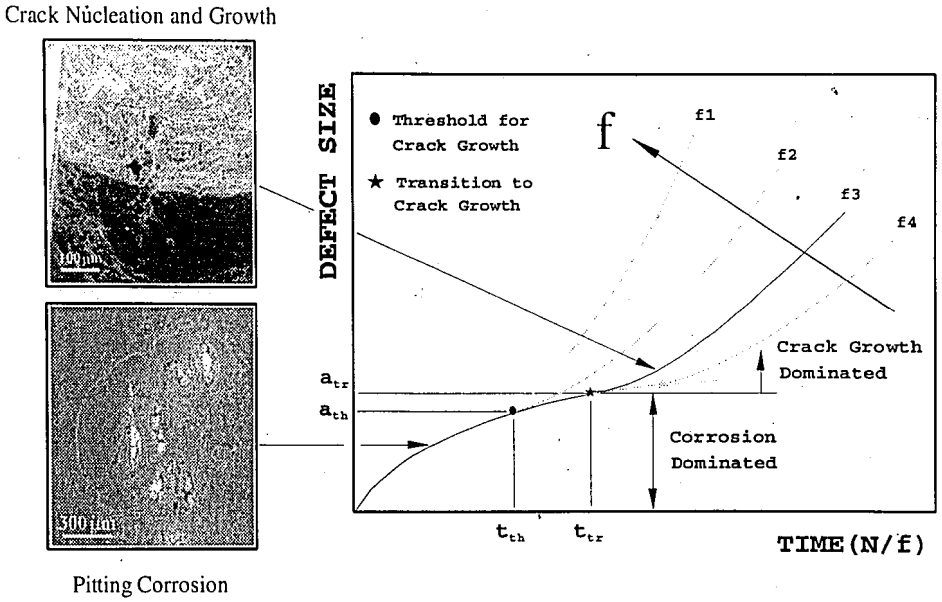

Figure 2.1 Schematic diagram of the development of corrosion fatigue from the evolution of pit in an aluminum alloy [9].

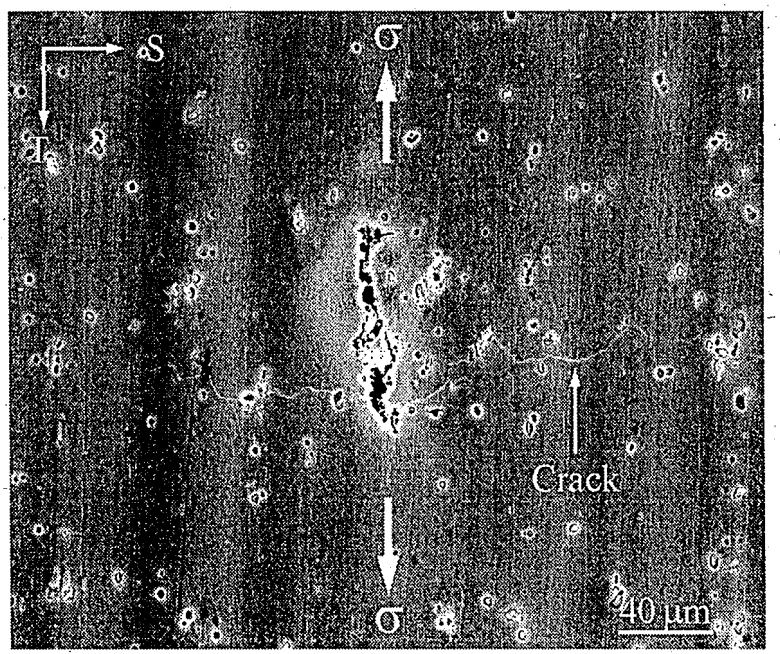

Figure 2.2 Pitting corrosion acting as crack nuclei in an aluminum alloy [9].

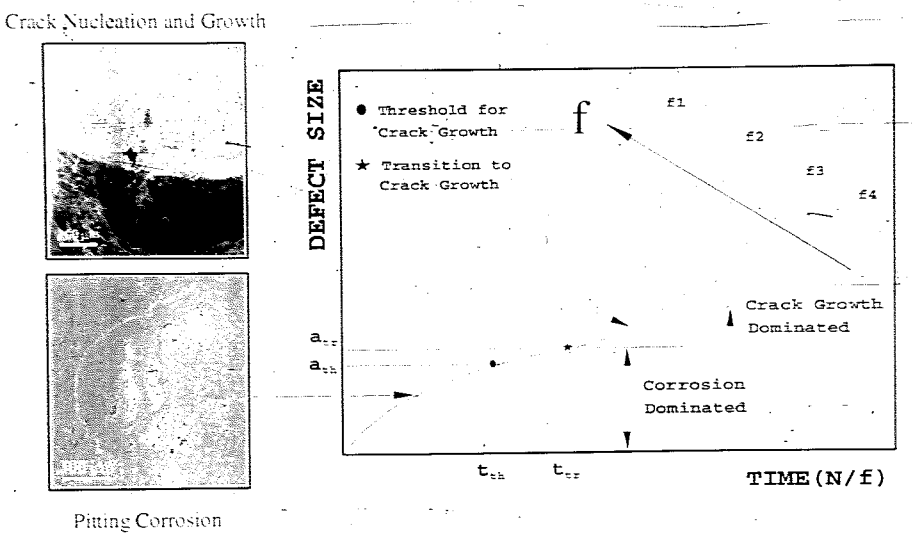

Figure 2.1 Schematic diagram of the development of corrosion fatigue from the evolution of pit in an aluminum alloy [9].

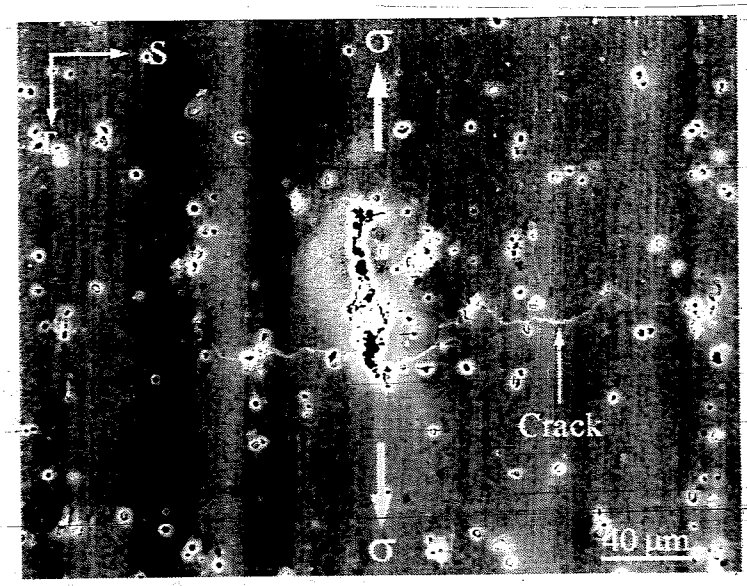

Figure 2.2 Pitting corrosion acting as crack nuclei in an aluminum alloy [9].

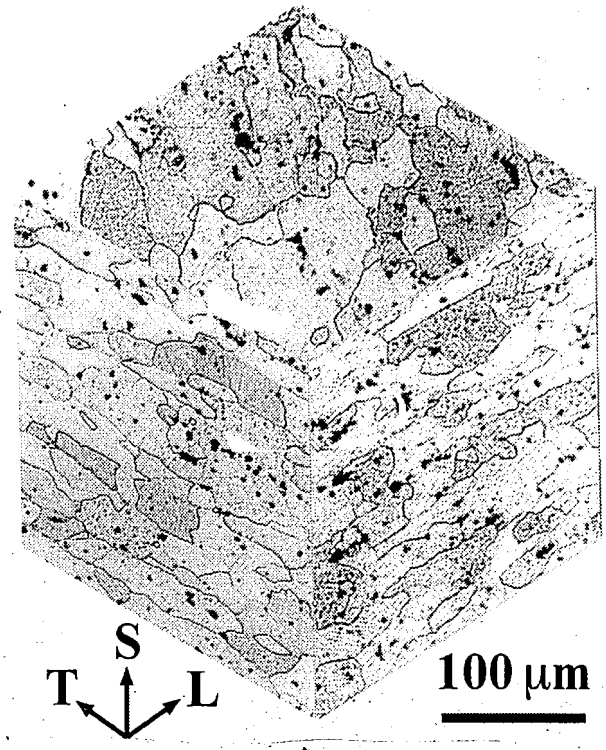

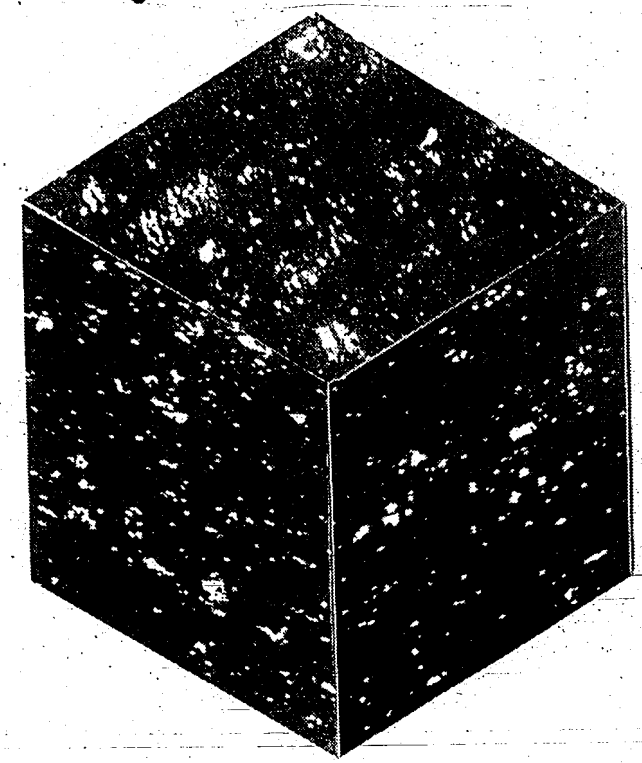

Figure 2.3 2024-T3 microstructure; distribution of grains (top) and distribution of constituent particles (bottom) [5].

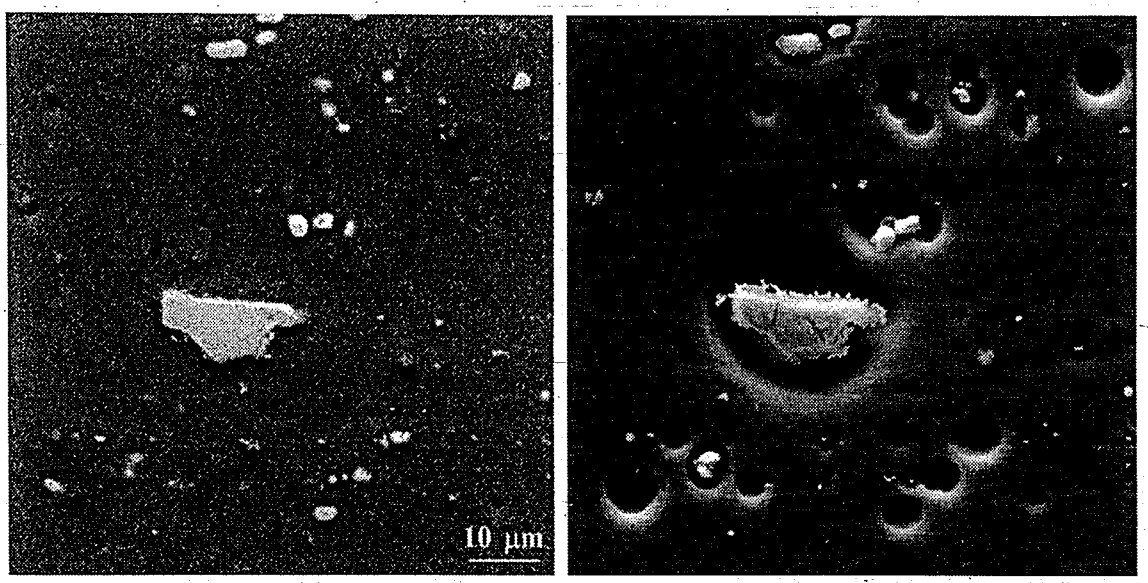

(a) (b)

Figure 2.4 Particle induced pitting corrosion in an aluminum alloy. The original surface is shown (a) and the surface after 24-hour corrosion time in (b) [9].

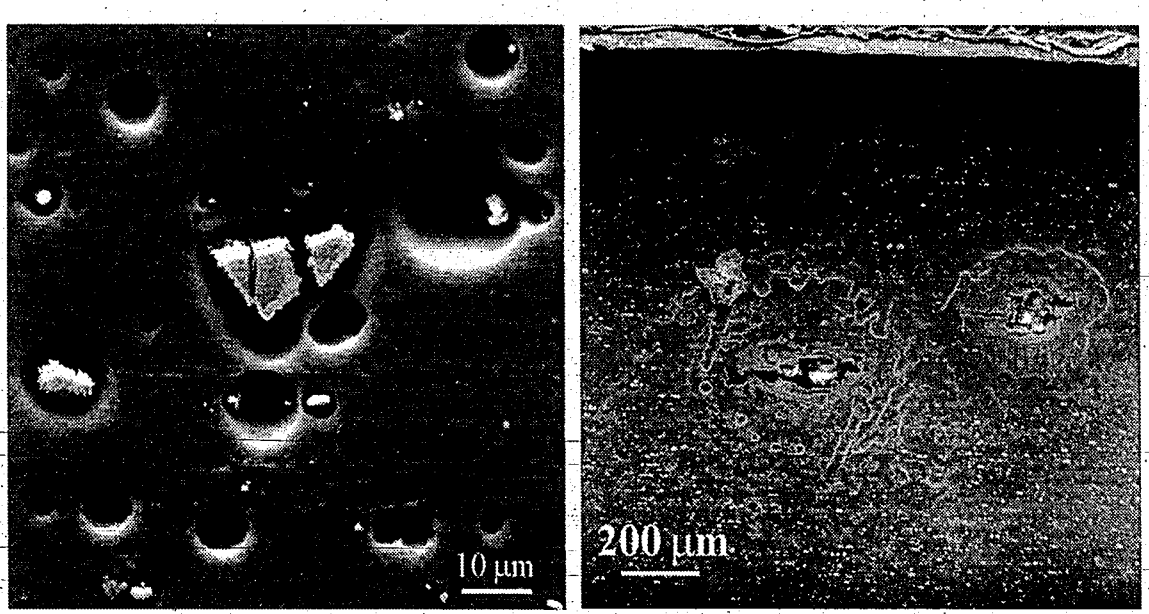

(a) (b)

Figure 2.5 Particle induced pitting corrosion showing (a) general pitting and (b) severe pitting [9].

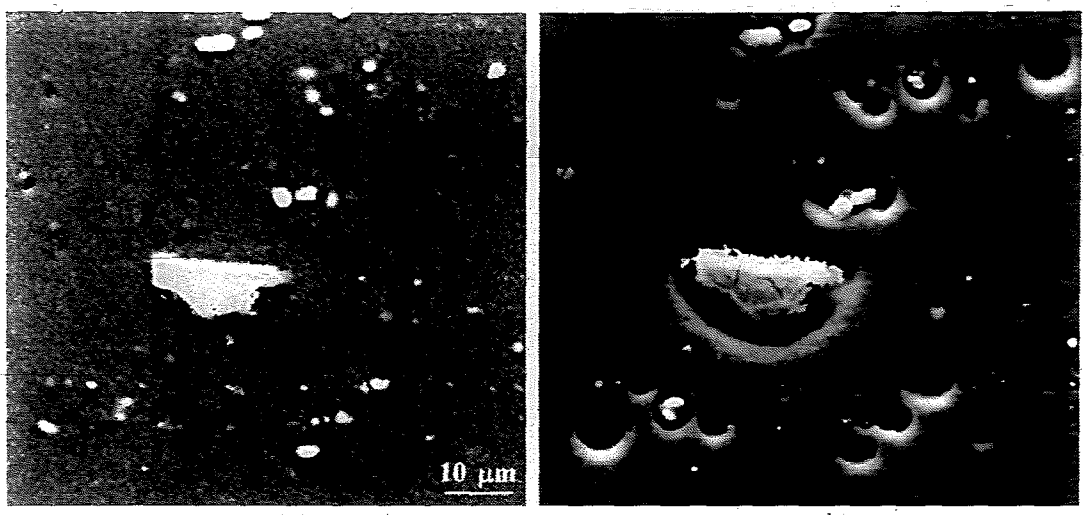

(a) (b)

Figure 2.4 Particle induced pitting corrosion in an aluminum alloy. The original surface is shown (a) and the surface after 24-hour corrosion time in (b) [9].

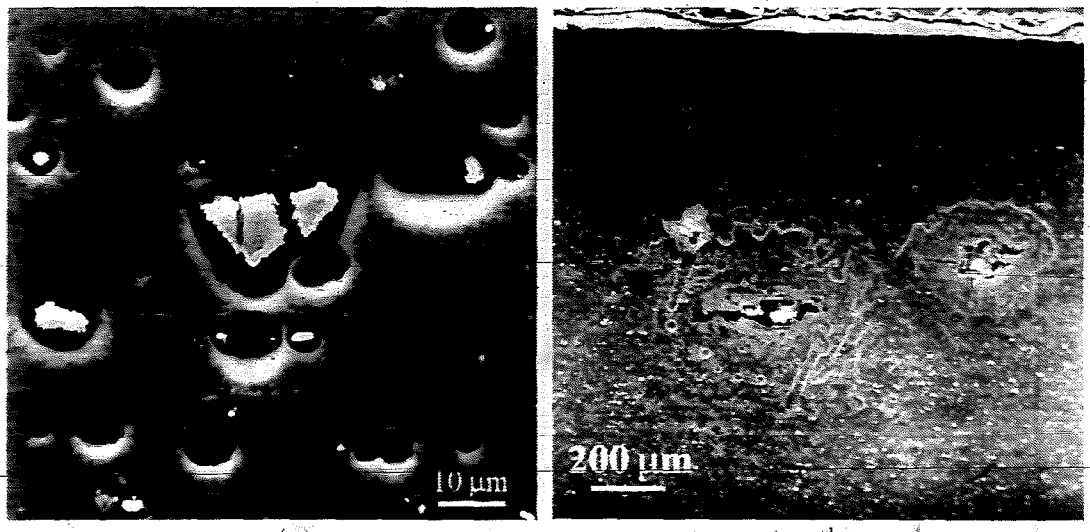

(a) (b)

Figure 2.5 Particle induced pitting corrosion showing (a) general pitting and (b) severe pitting [9].

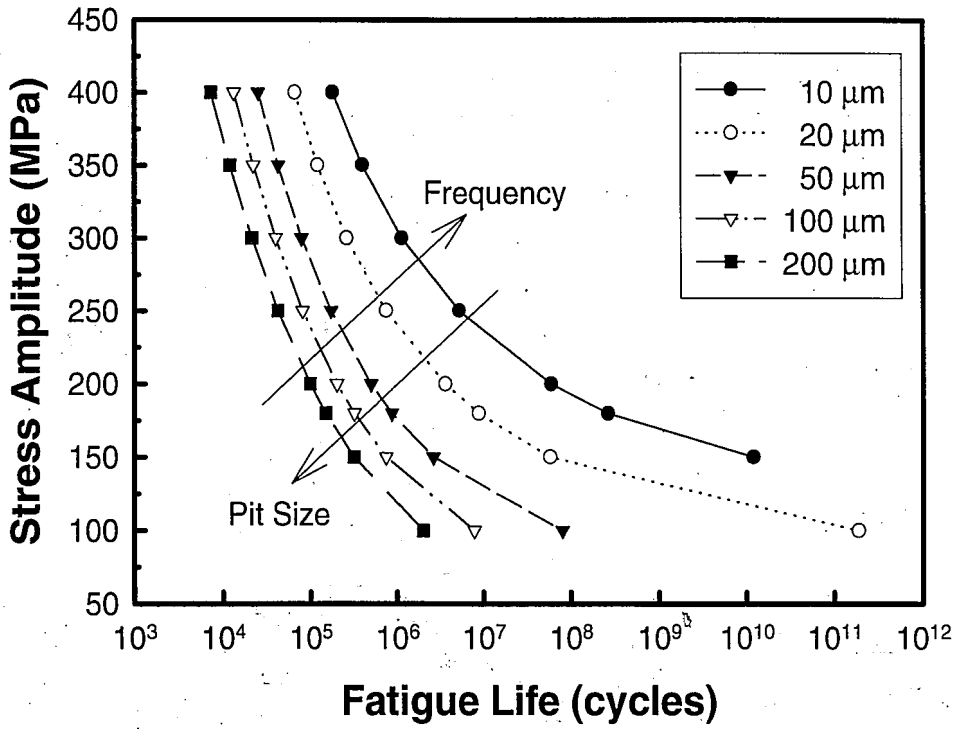

Figure 2.6 The influence of initial pit size and the reduction of fatigue life on the 2024-T3 aluminum alloy [33].

CHAPTER 3 EXPERIMENTAL STUDY

3.1 INTRODUCTION

The primary objective for this research is to determine if fatigue lives can be predicted from the initial pit size and the fatigue crack growth (FCG) properties. To achieve this objective, this research is divided into (i) experimental characterization of the effect of initial pre-corrosion pit of different sizes on fatigue behavior, (ii) measurement of pit size and correlation with fatigue life, and (iii) estimation of fatigue lives based on FCG. In this chapter, the material and the various experimental procedures are described.

3.2 MATERIAL

The material used in this experiment is a 1.6-mm-thick sheet of a high-strength 2024-T3 bare aluminum alloy. Because of its attractive properties, it has been widely used in structural components and other applications usually in the cladded form. The chemical composition, mechanical and corrosion properties of this alloy are listed in Table 3.1. Comparing 2024-T3 bare alloy to Alclad 2024-T3, this material is much more susceptible to a corrosion environment compared to Alclad 2024-T3 [35], so the surface will be rougher and have the multiple crack origin sites, when exposed to deleterious environment.

3.3 SPECIMEN

3.3.1 SPECIMEN DESIGN

Specimens were designed specifically to examine the effect of pre-existing corrosion pits on fatigue life in the long transverse or transverse longitudinal (T-L) orientation. Dimensions were 1.6 mm (0.063 in.), 177.8 mm (7 in.), and 25.4 mm (1 in.) of thickness, length, and width in gauge measurements, respectively. A semi-circular notch with radius of 3.175 mm (0.125 in.) along one edge of the specimen was used to simulate the geometrical stress concentration of rivet hole in aircraft fuselage and to facilitate the introduction of pre-corrosion. Specimen location and drawing are shown in Figure 3.1.

3.3.2 SPECIMEN PREPARATION

To minimize the influence of extraneous factor, the specimens were carefully prepared Specimens were machined to the specified dimensions by wire electro-discharge machining (EDM) to minimize residual stresses. The specimen edges and notches were polished through a series of silicon carbide (SiC) papers and pastes to #1500 grit and then polished with diamond paste to a 1 μm rms (root mean square) finish to minimize the presence of surface defects.

The notches were then pre-corroded in 0.5M NaCl solution (pH ≈ 6.5, dissolved oxygen concentration $[O_2] \approx 7$ ppm) at room temperature (~ 20°C) for 48 to 384 hours (2 to 16 days) to produce pits of a range of sizes. Each specimen was coated with stop-off lacquer leaving only the notch surface exposed.

3.4 EXPERIMENTAL APPARATUS

A computer-controlled closed-loop servo-hydraulic machine was used for the fatigue experiments. The machine calibration and load-train alignment were checked prior to testing. The calibration and alignment were demonstrated by using a calibration specimen attached with two strain gauges mounted on each side.

3.4.1 APPARATUS PREPARATION

A uniform stress distribution across the specimen cross-section was desired to ensure the absence of lateral bending and twisting. To ensure uni-axial tension-tension loading condition, the testing machine was aligned and calibrated [36]. In placing the specimen on the machine, an error limit of 0.0254 mm (0.001 in.) was used to minimize bending or torsional effect for accurate testing.

3.4.2 TESTING MACHINES

Specimens were tested in a 45 KN (10 Kip) MTS[1] machine at laboratory temperature. The main testing frame is composed of a closed-loop servo-hydraulic MTS testing machine with a FTA[2] interface. This machine is equipped with a MTS 458.20 MicroConsole, which responds to commands for axial cyclic loading. The main console that regulated the whole system using FTA control and data acquisition software is a PC (IBM PS/2 Model 30286), provides waveform signals to the servo-hydraulic machine, and acquires data on line.

[1] MTS System Corporation, Eden Prairie, MN 55344

[2] Fracture Technology Associates, Pleasant Valley, PA 18951.

3.5 Scanning Electron Microscope Observations

The fractographic studies were made by scanning electron microscopy (SEM) to correlate the fatigue behavior with corrosion pits at the notch surface. It was anticipated that the failure mode and the cracking mechanisms could be characterized by examining the post-fracture surface morphologies produced in laboratory environment. Information about the pre-existing corrosion pits on the fatigue lives can be obtained by comparing the surface morphologies of crack nucleation and propagation.

3.5.1 Preparation for SEM

Fractographic examinations may be hampered by the corrosion products (aluminum oxide) that form in the notch area during pre-pitting. As such, a two-step procedure was used to facilitate fractography. Frist, corrosion product on the notch surface was partially removed by the dry stripping method using an acetate replicating tape. Repeated stripping produced a reasonably clean notch for further chemical cleaning.

The cleaning solution was prepared by mixing 17.5 ml of phosphoric acid (H_3PO_4) and 5 g of chromic trioxide (CrO_3) with deionized water to produce 1000 ml of solution [37]. Specimens were fully cleaned in the cleaning solution at 55°C for 10 minutes. Trial experiments were conducted and demonstrated that this chemical cleaning did not induce significant further corrosion. This procedure was effective in removing the corrosion products [9].

3.5.2 FRACTOGRAPHIC STUDIES

The fractographic examinations were conducted to determine the crack nucleation site and the size and geometry of a crack nucleating corrosion pit. An optical microscope was first used to gain an overall perspective of the crack nucleation and propagation behavior. An ETEC SEM, operated in the secondary electron (SE) imaging mode at 20 KV with a working distance of about 30 mm, to develop detailed information about the crack nucleating sites. Mating surfaces were examined to further study the micromechanisms for fatigue cracking.

Table 3.1 (a) Chemical composition and (b) mechanical and corrosion properties of a 2024-T3 aluminum alloy [38].

(a) Chemical Composition

Weight Percent								
Cu	Mg	Mn	Fe	Zn	Si	Ti	Cr	Al
4.24	1.26	0.65	0.15	0.08	0.06	0.031	<0.01	Balance

Analyzed by Laboratory Testing Inc., P.O. Box 249, Dublin, PA 18917.

(b) Mechanical and Corrosion Properties

Tensile Strength[1]	480 MPa
0.2% Offset Yield Strength[1]	355 MPa
Elongation[2]	17%
Modulus of Elasticity[2]	72.4 GPa
Poisson's Ratio[2]	0.33
Free Corrosion Potential (SCE)[3]	-600/-800 mV (aerated/deaerated soln.)

[1] Tested by Laboratory Testing Inc., P.O. Box 249, Dublin, PA 18917;
[2] ASM Specialty Handbook: Aluminum and Aluminum Alloy, ASM International, 1993;
[3] Measured in this study, in agreement with available data (aerated soln.) in [2].

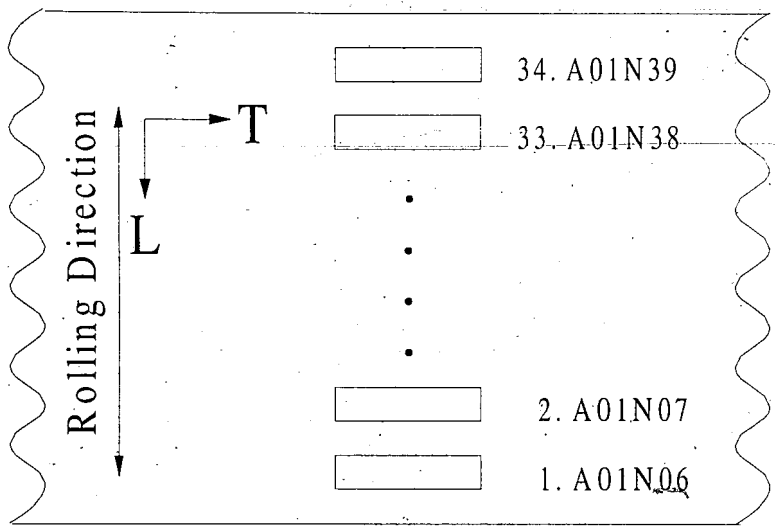

(a)

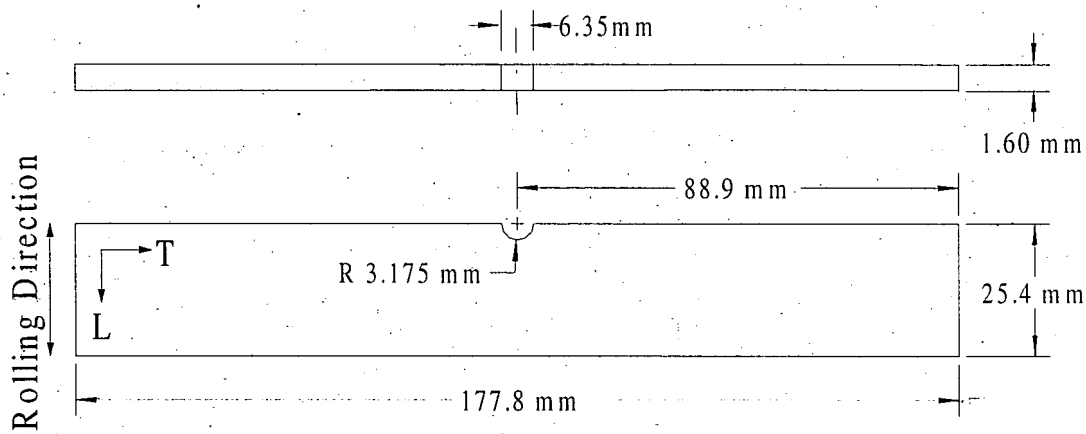

(b)

Figure 3.1 (a) The location of test specimens in the original sheet and (b) fatigue specimen geometry and orientation (T-L).

CHAPTER 4 EXPERIMENTAL RESULTS

4.1 INTRODUCTION

This chapter describes the results of fatigue experiments and fractographic examinations of the fracture surfaces. Fatigue experiments were performed on pre-pitted single edge notch (SEN) specimens of a 2024-T3 aluminum alloy as a function of pre-corrosion time. Post-fracture fractographic examinations were made by optical microscopy (OM) and scanning electron microscopy (SEM) to determine the origin of fatigue failure and its geometry and size.

4.2 FATIGUE EXPERIMENTS

The results on SEN specimens, with a semi-circular edge notch that had been pre-pitted in a 0.5M NaCl solution (pH ≈ 6.5, $[O_2]$ ≈ 7 ppm) for 48 to 384 hours (2 to 16 days) and fatigue tested in laboratory air, are presented. For comparison and further analysis, previous test results on central circular-hole (CCH) specimens of the same alloy [11] were also included. The applied loads for each specimen were adjusted to produce a stress of $k_t\Delta\sigma$ of 288 MPa (R = 0.1) at the notch root where k_t represents the elastic stress concentration factor and $\Delta\sigma$ the remote cyclic stress range.

4.2.1 TEST RESULTS ON SEN SPECIMENS

The fatigue test results on SEN specimen that had been pre-pitted (pre-corroded) for 48 to 384 hours (2 to 16 days) in a 0.5M NaCl solution are given in Table 4.1 and are also shown in Figure 4.1. A specimen, without prior corrosion, was used as reference.

This specimen exhibited a fatigue life of more than 2.5 million cycles, which is indicative of the inherent fatigue life of this alloy in air at $k_f\Delta\sigma$ of 288 MPa.

Overall, the fatigue lives decreased with increasing time of pre-pitting. The more than one order of magnitude reduction in life generally reflected the expected deleterious influence of pitting damage [5,7,9,10,12,16,18,24,28,30,31]. Considerable variability in fatigue lives, however, was observed. The degree of variability decreased with increasing pre-pitting time. For example, the fatigue lives of specimens pre-pitted for 48 hours varied from 158,000 cycles to over 2 million cycles. Similar variability was observed at the longer pre-pitting times; namely, from about 150,000 to 339,000 cycles at 96 hours, from about 125,000 to 198,000 cycles at 192 hours, and from about 106,000 to 171,000 cycles at 384 hours. These observations are consistent with the results of Harmsworth [10] on a 2024-T4 alloy tested in rotating bending, and confirm the role of prior corrosion damage (pitting) in reducing fatigue lives.

Because the size and location of corrosion pits at a given time are expected to be randomly distributed, the variability in fatigue lives at a prescribed pre-pitting time may reflect the distribution in sizes of crack nucleating pits. It might be more appropriate, therefore, to correlate the changes in fatigue life with pit size rather than pre-pitting time. This possibility will be considered following the fractographic examinations of the crack nucleation sites.

4.2.2 Prior Result on Central Circular-Hole Specimens

As a part of this examination, previous measurements of fatigue lives as a function of pre-pitting time for central circular-hole (CCH) specimens of the same 2024-

T3 alloy, under the same set of testing conditions, are included. The CCH specimens are 1.6 mm thick, with a 177.8 mm long by 30.5 mm wide gauge section that contains a central circular hole of 5.35 mm radius. The CCH specimens differ from the SEN specimens in that the loading is symmetrical and the probable location for crack nucleation is doubled.

Results from this experiment are given in Table 4.2 and the fatigue lives for the SEN and CCH specimens are shown together as a function of pre-pitting times in Figure 4.2. The overall trend in the data is consistent with those of the SEN specimens, with decreasing fatigue lives at the longer pre-pitting times. The variability in fatigue lives at a given pre-pitting time appears to be greater. With no pre-pitting or at short exposure times, the fatigue lives exceeded 2 million cycles, although some fatigue lives ranged from 165,000 to 240,000 cycles.

For the 100-hour pre-pitted specimens, the fatigue lives ranged from 130,000 to 406,000 cycles versus 150,000 to 340,000 (at 96 hours) for the SEN specimens. This apparent difference may reflect the distribution in the sizes of crack nucleating pits, and will be considered on the basis of the fractographic examination.

4.3 FRACTOGRAPHY

Optical microscopy (OM) and ETEC scanning electron microscopy (SEM) were used to identify and characterize the origins for fatigue failure by post-fracture examinations of the fatigue-fracture surfaces. The examinations were focused on the region near the notch surfaces, and were directed toward the identification of the crack nucleation site, the sizes of each corrosion pit, the dominant pit in each specimen, and

other potential crack nuclei. Mating fracture surfaces, and the fracture surfaces were viewed with and without tilting to better identify the crack nuclei and their size and shape. To focus upon failure that nucleated from corrosion pits, other causes for crack nucleation were first identified.

4.3.1 Failure by Other Causes

Based on the fractographic examinations, three types of nucleation sites are eliminated from further analyses; namely, nucleation from (i) prior mechanical damage (ii) large constituent particles, and (iii) corrosion pits away from the notch surface.

4.3.1.1 Mechanical Damage

The first type is prior mechanical damage on the specimen. In Figure 4.3, a specimen (A01N58) pre-corroded for 48 hours with fatigue life of 159,000 cycles, notch indicated a direction of thickness, S (surface) orientation, and side represented a rolling direction, L (longitudinal) orientation. From the evidence of river flow patterns that implied dominant defects on the fracture surface, tear-like prior mechanical damage was found on the side. A mark of 0.15 mm wide band near T (transverse) orientation, perpendicular to L orientation, was revealed resulting in a severe damage close to the notch in section ***A***. A two-layered-like fracture at high magnification of section ***A*** indicated that there were no symptoms of corrosion pitting. Similar to this result, another one showed an equivalent failure in a specimen (A01N11) pre-corroded for 96 hours with a fatigue life of 150,000 cycles.

4.3.1.2 PARTICLE NUCLEATED FATIGUE FAILURE

The second type is a particle nucleated fatigue failure on a specimen (A01N46) pre-corroded for 48 hours with a fatigue life of 158,000 cycles. In Figure 4.4, the river flow patterns in the form of peaks and gorges converging toward the crack nucleation site ***A*** on the left, which in turn, showing in reverse the direction of crack propagation. Conversely, area ***B*** represents a series of peaks toward the crack propagation direction, which hindered crack propagation and leaving wedges on the side, with no evidence of crack nucleation. With this evidence, the particle was shown in a shape of semi-ellipsoid, 18.2 μm wide by 35.2 μm deep in size, on the right and was identified as the dominant crack nucleus for fatigue failure. Because this study was focused primarily on corrosion pits so that this case was eliminated from further analysis.

4.3.1.3 CORROSION PIT OUTSIDE OF NOTCH

The third type is a corrosion pit away from the notch surface. Figure 4.5 shows crack nuclei on the fracture surface and at a higher magnification. The appearance of the nuclei suggests that fatigue cracking is associated with two large constituent particles, linked by a corrosion pit. This type of crack nuclei was observed in two specimens, one (A01N52) pre-corroded for 48 hours, with fatigue life of 436,470, and the other (A01N29) pre-corroded for 96 hours, with fatigue life of 338,690. These specimens contributed to the large scatter in fatigue lives in Figure 4.1. Because crack nucleation did not occur from the notched surface, the specimens were not considered for further analysis. Their contribution to the overall distribution of fatigue lives, however, needs to be considered in design and reliability analysis.

4.3.2 Dominant Pit and Pit Size Measurement

The remaining specimens, after removing those that have failed by the other causes, were examined to identify and characterize the dominant pit at single and multiple crack nucleation sites in SEN and CCH specimens by scanning electron microscopy (SEM). Mating fracture surfacces were used to aid in the identification and characterization. Overlays semi-ellipse were used with micrographs of corrosion pits to provide more accurate measurements of their size.

4.3.2.1 Dominant Pit in SEN Specimens

As pre-corrosion time increased, the SEM fractographs showed a change from crack nucleation at a single corrosion pit to multiple site nucleation. Figure 4.6, for a specimen (A01N39) pre-corroded for 384 hours, with fatigue life of 171,000 cycles, shows two nuclei (or pits) , and is used to illustrate the procedure for identifying the dominant corrosion pit for crack nucleation. The identification procedure involved an examination of the pattern of crack growth away from the crack nuclei, and a comparison of the size of the candidate corrosion pits. From the overall crack growth (river) patterns, Figure 4.6 (a), the crack nuclei are expected to be found in flat surface area on the left side of the micrograph. The two candidate nuclei are identified as corrosion pits located at ***A*** and ***B***. More detailed examinations show the growth pattern from ***A*** as marked in Figure 4.6 (b) is broader than that from ***B*** and suggests ***A*** as the dominant pit. This is confirmed by the fact that the pit at ***A*** is larger than the one at ***B***; 20 μm wide by 25 μm deep versus 11 μm wide by 16 μm deep (compare Figure 4.6 (c) and (d)).

Following the same procedure, the dominant corrosion pits at the various pre-corrosion time were identified. Examples of these pits are shown in Figure 4.7: (a) a specimen (A01N06) pre-corroded, for 384 hours, with a 20 μm wide by 54 μm deep pit, (b) a specimen (A01N34), for 192 hours, with a 25 μm wide by 27 μm deep pit, and (c) a specimen (A01N07), for 96 hours, with a 18 μm wide by 25 μm deep pit.

In some cases, the dominant pit (or crack nuclei) is at the edge of the notch. Here, the pit would be modeled as corner crack in the form of a quarter ellipse. Representative nuclei are shown in Figure 4.8 for a specimen (A01N21) pre-corroded for 384 hours and a specimen (A01N14) pre-corroded for 192 hours.

4.3.2.2 Dominant Pit in CCH Specimens

For the central circular-hole (CCH) specimens, fatigue cracking can begin from either or both sides of the hole. Identification of the dominant pit, therefore, entails fractographic examinations of the crack surfaces on both sides. Figure 4.9, for a specimen (O13) pre-corroded for 24 hours, with fatigue life of 173,300 cycles, show two sets of candidate nuclei on both sides. Following the previous procedure that can identify the dominant pit, the pit (12.77 μm wide by 20.11 μm deep) at ***A*** in (c) is identified as the dominant one of the pair, ***A*** and ***B***, since cracking associated with the pit at ***A*** covered most of the fracture surface, Figure 4.9 (a), with a ridge ***C*** between two different crack planes. On the other side, crack nuclei at ***D*** and ***E***, Figure 4.9 (b), appear to have contributed to crack propagation together. More detailed examinations show the growth pattern from ***D*** is similar to that of ***E***. The pit at ***D*** (Figure 4.9 (d)), however, is much larger than the one at ***E*** (20.65 μm wide by 44.65 μm deep versus 6.59 μm wide by 18.84

μm deep), and is taken as the dominant pit. Even though the pit at ***D*** is larger than that at ***A***, the limited extent of fatigue cracking on the ***D*** side suggests that the pit at ***A*** was the dominant nucleus. Most specimens followed the same procedure except a 24-hour pre-corroded specimen (O8) that had corrosion pits on only one side.

4.3.2.3 Pit Size Measurement

All of the pits on the fracture surfaces were measured from the SEM micro-fractographs by assuming that the pits act as equivalent semi-elliptical surface cracks. Measurements were made by matching semi-ellipses (Figure 4.10) to the fractographs, and assuming by matching quarter-ellipses to the corner cracks. Estimates of the upper and lower bounds for the dominant corrosion pit in each specimen were obtained and are recorded in Tables 4.3 and 4.4 for the 2024-T3 SEN specimens and in Table 4.5, for the CCH specimens.

4.4 Correlation of Fatigue Life with Pit Size

Based on these measurements, the data on observed fatigue lives of 2024-T3 SEN specimen, shown in Figure 4.1 are replotted as a function of pit depth in Figure 4.11, and together with the results on CCH specimen in Figure 4.12. The changes of fatigue lives are seen to be better correlated with the pit depth than pre-corrosion time (*cf*, Figures 4.1 and 4.2). The observed variability reflects errors in pit size measurement and the influence of aspect ratio of the nucleating corrosion pit. The possibility will be considered in the following chapter.

Table 4.1 Experimental fatigue result for the SEN specimens at $k_t\Delta\sigma$ = 288 MPa, R = 0.1 and f = 30 Hz.

Specimen Number	Specimen Location	Pre-Corrosion Time (hours)	Fatigue Life (cycles)
A01N22	17	0	2,500,000[1]
A01N20	15	48	1,547,492[1]
A01N27	22	48	1,999,968[1]
A01N44	5	48	2,066,597[1]
A01N49	10	48	1,495,592[1]
A01N58	19	48	158,752[2]
A01N11	6	96	149,765[2]
A01N46	7	48	157,796[3]
A01N52	13	48	436,471[4]
A01N29	24	96	338,687[4]
A01N17	12	48	304,594
A01N18	13	48	187,144
A01N07	2	96	153,691
A01N15	10	96	132,808
A01N36	31	96	158,056
A01N12	7	192	159,106
A01N14	9	192	160,121
A01N19	14	192	198,381
A01N23	18	192	134,965
A01N34	29	192	125,216
A01N06	1	384	106,318
A01N21	16	384	162,567
A01N30	25	384	142,584
A01N32	27	384	120,168
A01N39	34	384	171,078

[1] Test terminated without failure.
[2] ≡ specimen had mechanical damage.
[3] ≡ fatigue failure nucleated at a constituent particle.
[4] ≡ the dominant pits were outside of the notch.

Table 4.2 Experimental fatigue result for the CCH specimens at $k_t\Delta\sigma$ = 288 MPa, R = 0.1 and f = 30 Hz.

Sample Number	Pre-Corrosion Time (hours)	Fatigue life(cycles)
C12	0	1,983,885[1]
C5	0	2,000,153[1]
O1	10	1,180,641[1]
C11	10	1,624,860[1]
C7	24	2,129,225[1]
O9	10	165,244
O8	24	239,202
O13	24	173,306
C8	100	405,784
C1	100	129,556
C9	100	354,830

[1] Test terminated without failure.

Table 4.3 Upper and lower bounds of initial crack sizes on the notch surface for the SEN specimens at $k_t\Delta\sigma = 288$ MPa, $R = 0.1$ and $f = 30$ Hz.

Specimen Number	Corrosion Time (hours)	Observed Fatigue Life(cycles)	Tensile Mode (mm)	c (μm)	a (μm)	c/a
A01N17	48	304,594	3.0	4.25	19.14	0.22
A01N18	48	187,144	2.5	5.16	14.12	0.37
A01N46	48	157,796	4.0	9.35	18.07	0.52
A01N07	96	153,691	3.2	13.86	22.74	0.61
				18.05	25.07	0.72
A01N15	96	132,808	3.8	9.48	15.50	0.61
				10.99	17.15	0.64
A01N12	192	159,106	2.0	16.01	17.98	0.89
				26.76	17.24	1.55
A01N19	192	198,381	4.5	11.79	30.47	0.39
A01N23	192	134,965	3.1	12.34	15.13	0.82
				24.07	26.09	0.92
A01N34	192	125,216	2.8	20.14	26.72	0.75
				24.64	26.71	0.92
A01N06	384	106,318	2.0	18.84	33.65	0.56
				20.14	54.37	0.37
A01N39	384	171,078	4.0	19.43	23.25	0.84

Table 4.4 Experimental results of initial crack sizes at the corner of the notch for the SEN specimens at $k_t\Delta\sigma = 288$ MPa, $R = 0.1$ and $f = 30$ Hz.

Specimen Number	Corrosion Time (hours)	Observed Fatigue Life(cycles)	Tensile Mode (mm)	c (μm)	a (μm)	c/a
A01N36	96	158,056	3.9	30.55	33.35	0.92
A01N14	192	160,121	3.5	35.34	22.80	1.55
A01N21	384	162,567	3.5	25.53	43.15	0.59
A01N30	384	142,584	4.0	45.81	41.94	1.09
A01N32	384	120,168	6.5	50.89	52.46	0.97

Table 4.5 Experimental results of dominant crack sizes on both surfaces of the hole for the CCH specimens at $k_t\Delta\sigma = 288$ MPa, $R = 0.1$ and $f = 30$ Hz.

Specimen Number	Corrosion Time (hours)	Observed Fatigue Life(cycles)	Fracture Surface Feature	Tensile Mode (mm)	c (μm)	a (μm)	c/a
O8	24	239,202	Flat	5	5.00	20.39	0.25
O13	24	173,306	Flat	4	12.77	20.11	0.63
			Serrated	1	20.65	44.65	0.46
C1	100	129,556	Flat	2	10.59	23.42	0.45
			Serrated	2	11.00	16.02	0.69
C8	100	405,784	Flat	3	6.83	12.29	0.56
			Serrated	0	11.61	43.37	0.27
C9	100	354,830	Flat	2	7.79	14.87	0.52
			Serrated	0	6.26	51.48	0.12

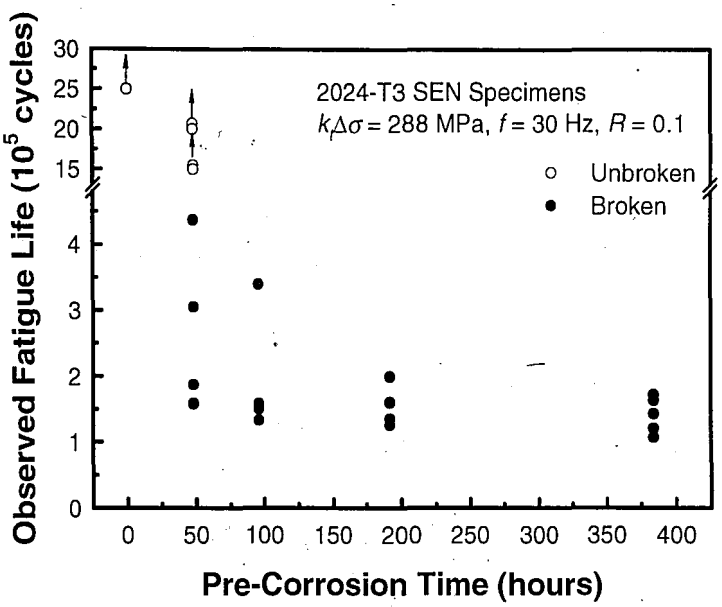

Figure 4.1 Reduction of fatigue life for 2024-T3 SEN specimens as a function of pre-corrosion time.

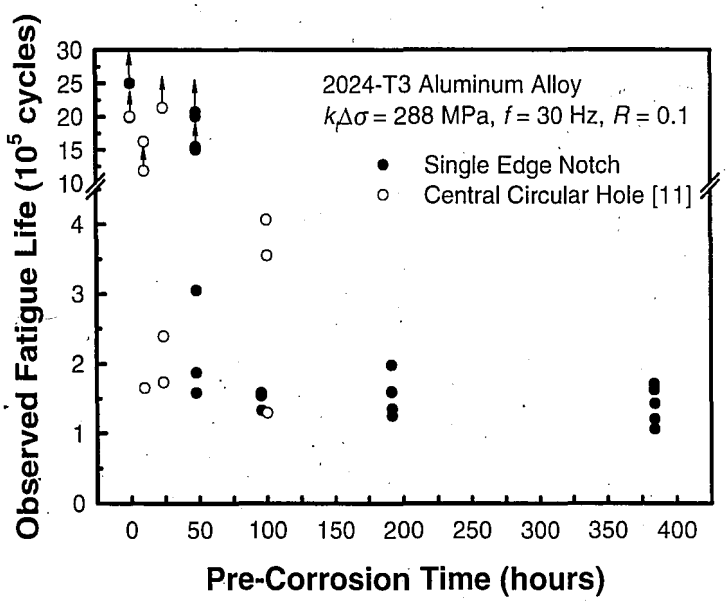

Figure 4.2 Reduction of fatigue life for 2024-T3 SEN and CCH specimens as a function of pre-corrosion time.

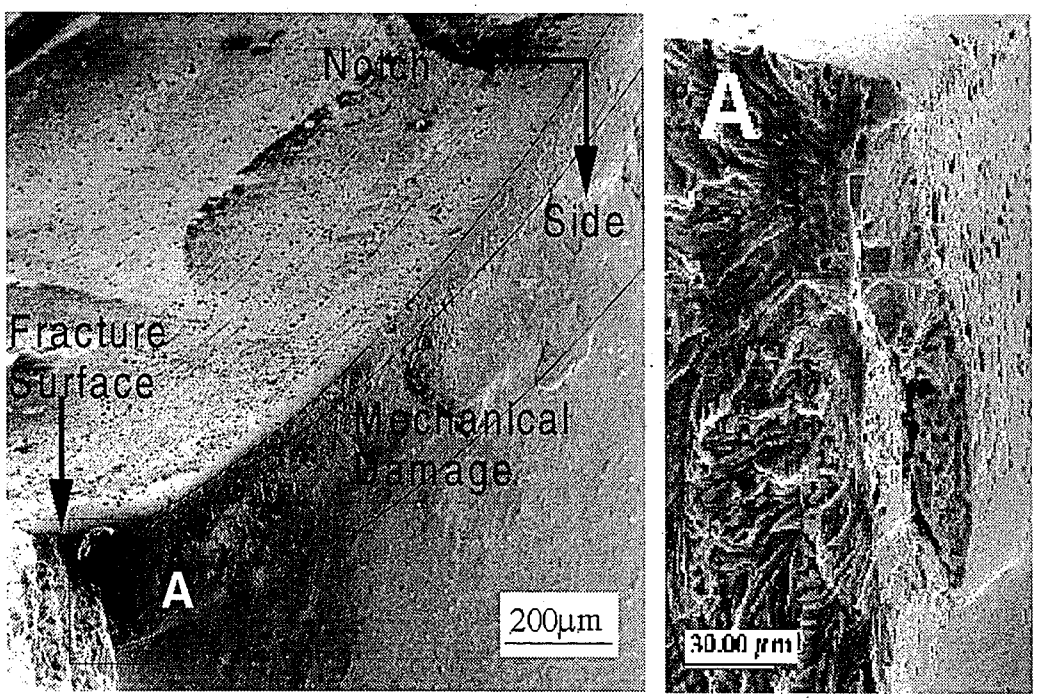

Figure 4.3 Mechanical damage present prior to pre-corrosion on a SEN specimen; 48-hour pre-corroded (A01N58).

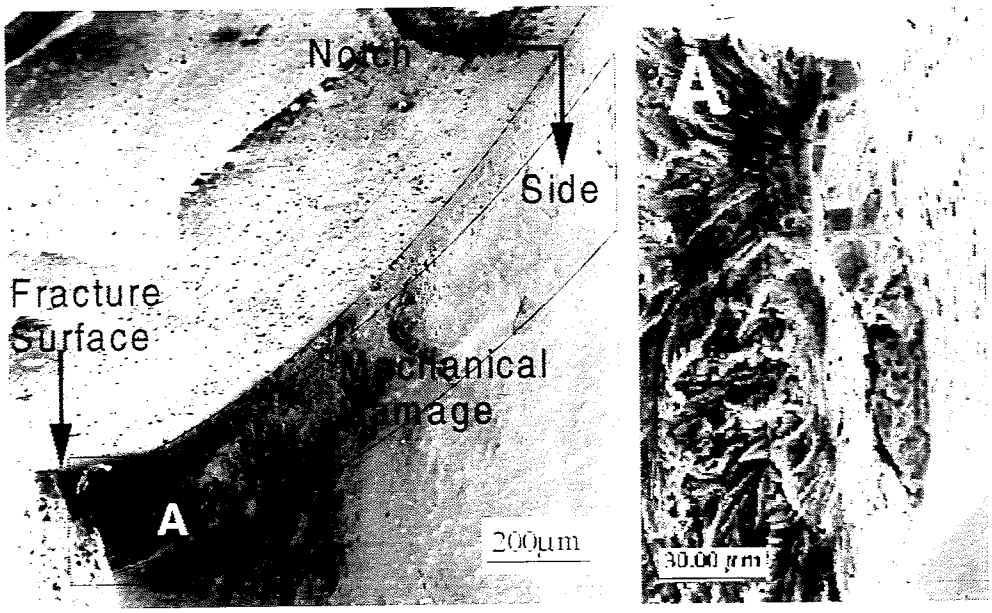

Figure 4.3 Mechanical damage present prior to pre-corrosion on a SEN specimen: 48-hour pre-corroded (A01N58).

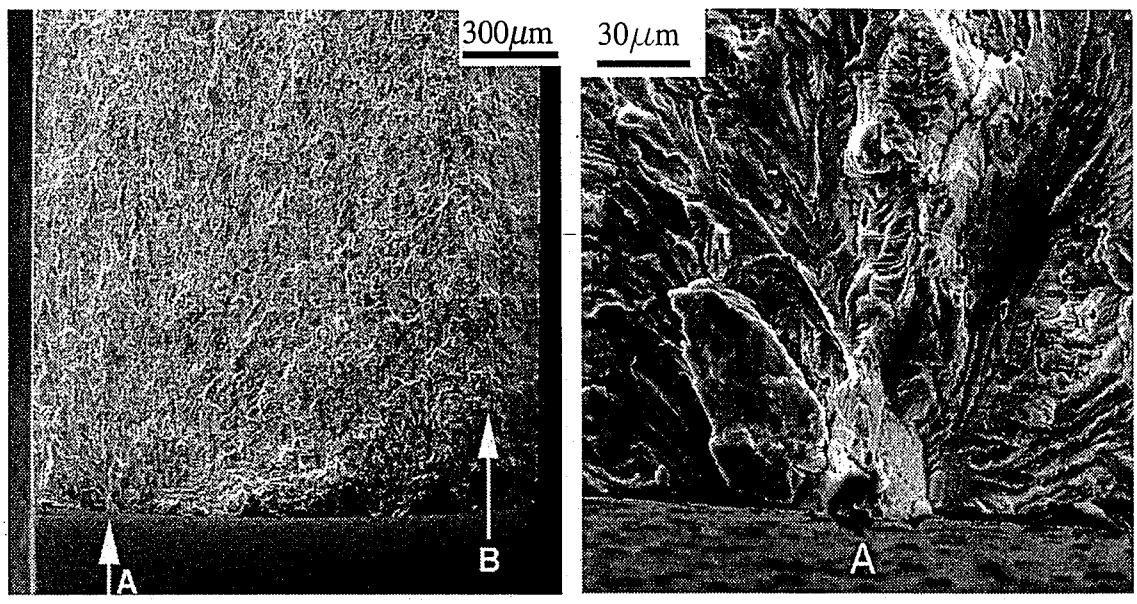

Figure 4.4 Fatigue crack initiation at a constituent particle in a specimen (A01N46) pre-corroded for 48 hours.

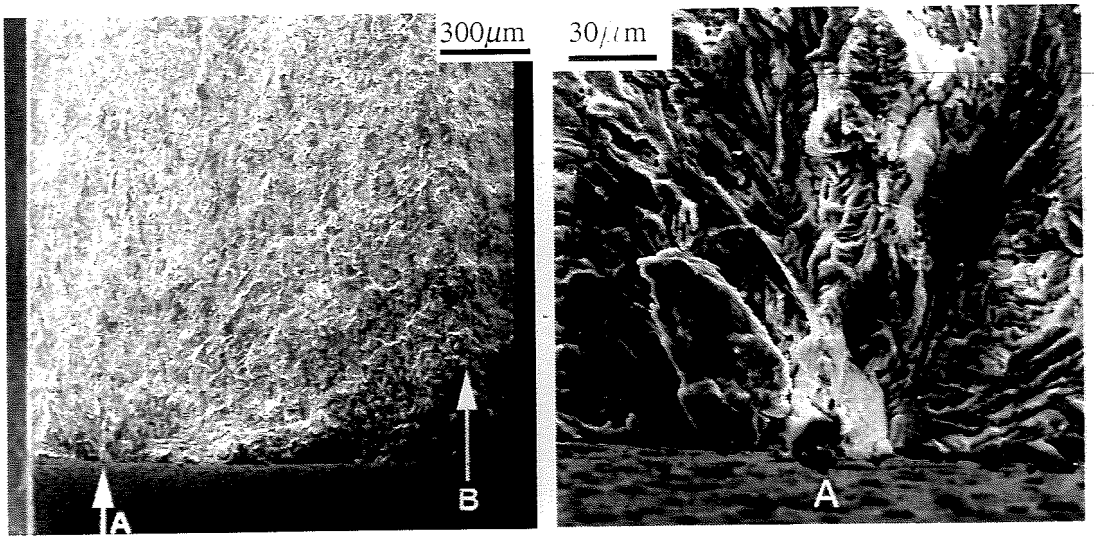

Figure 4.4 Fatigue crack initiation at a constituent particle in a specimen (A01N46) pre-corroded for 48 hours.

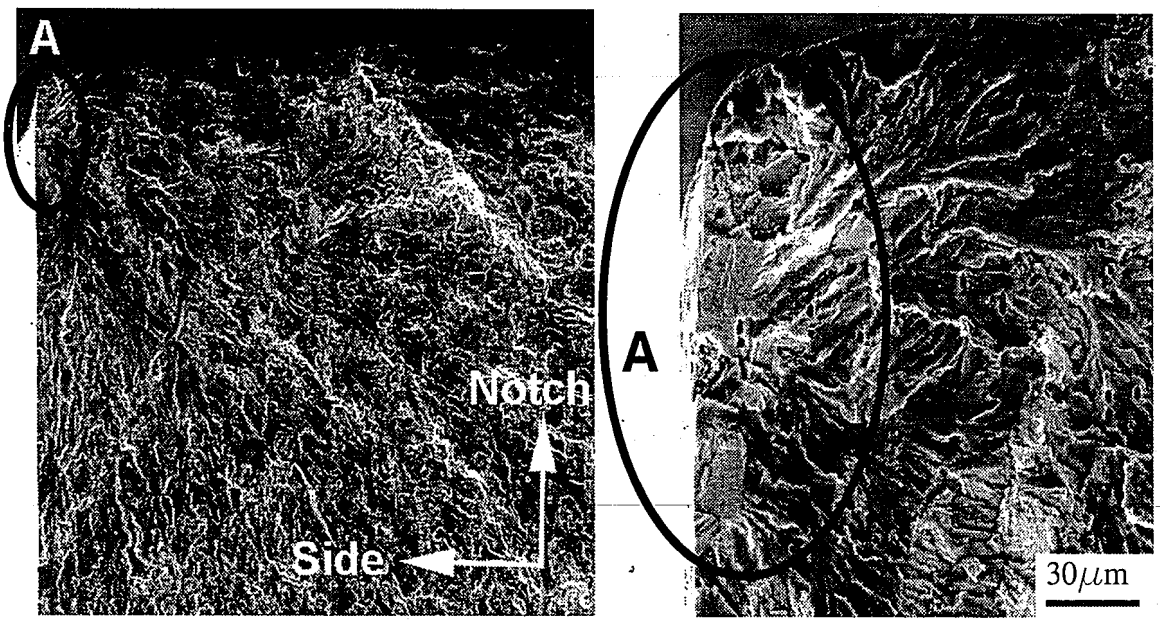

Figure 4.5 Fatigue crack initiation that occurred outside of the notch in a specimen (A01N52) pre-corroded for 96 hours.

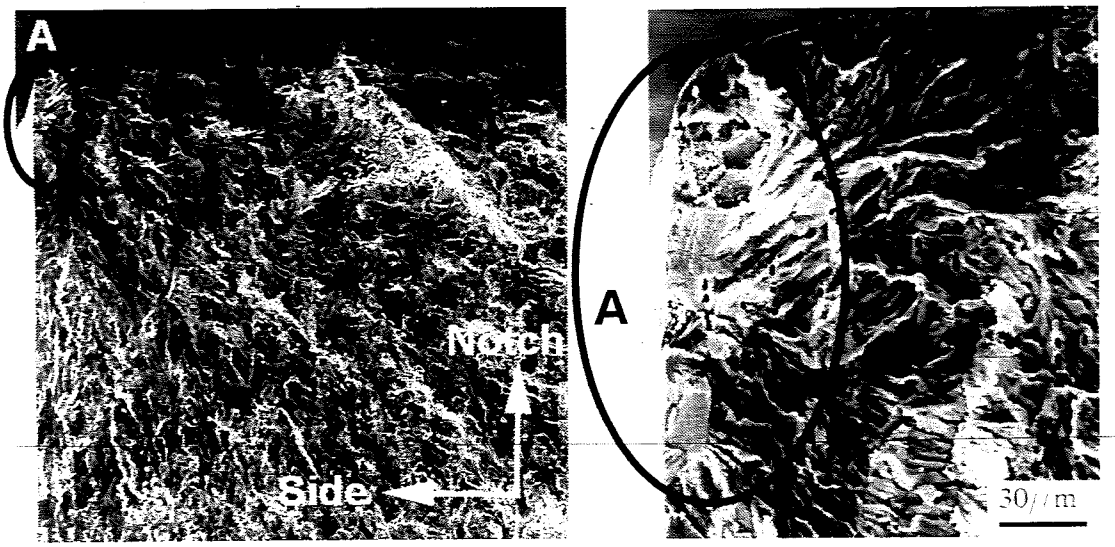

Figure 4.5 Fatigue crack initiation that occurred outside of the notch in a specimen (A01N52) pre-corroded for 96 hours.

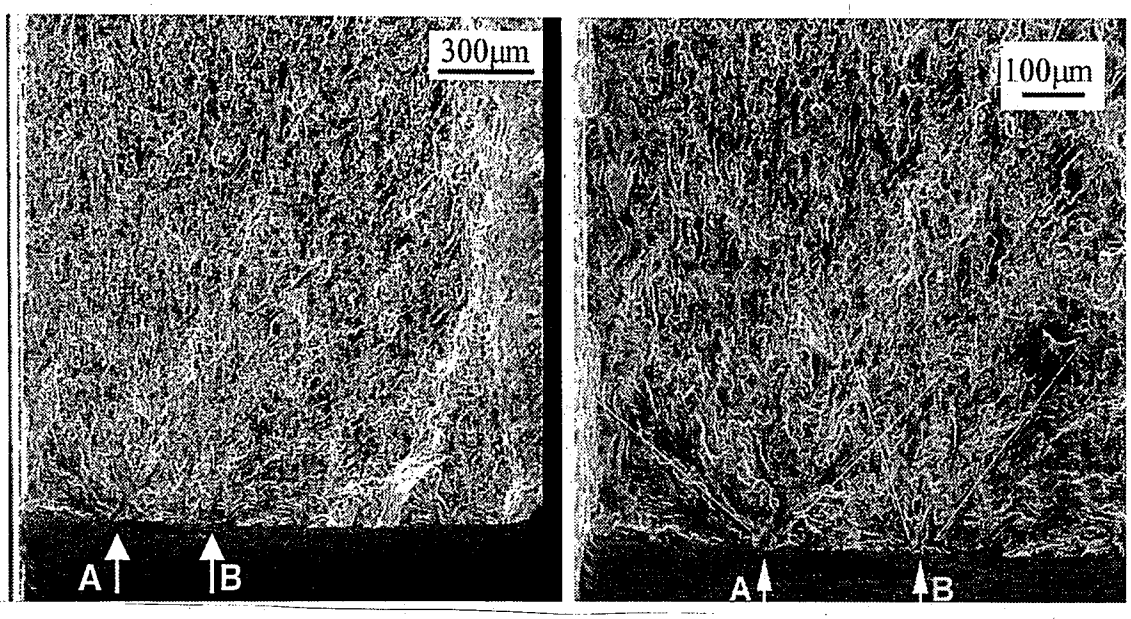

(a) (b)

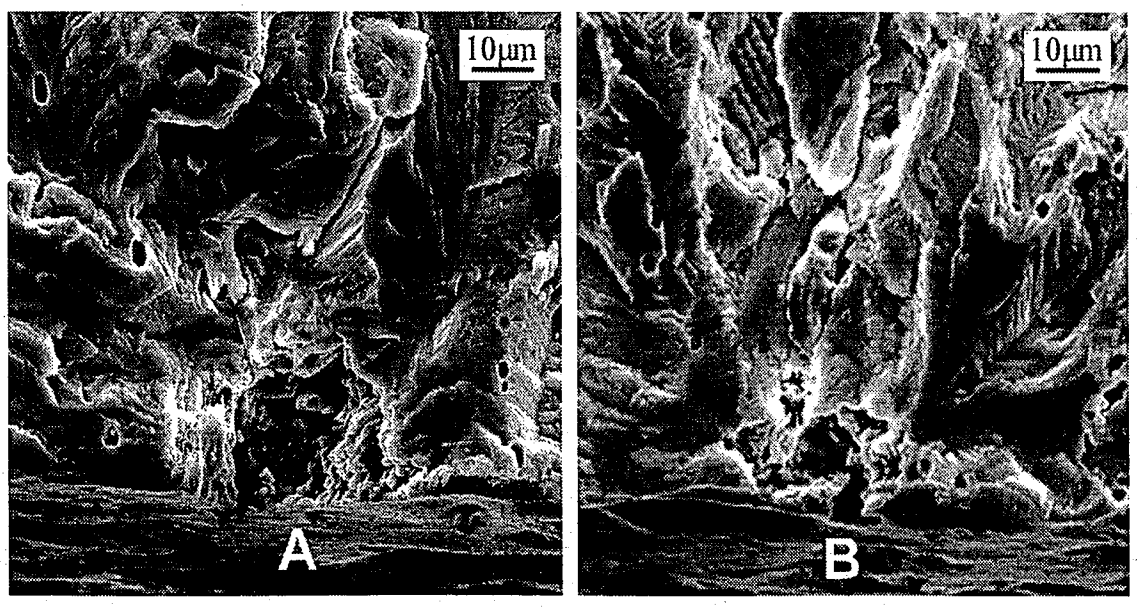

(c) (d)

Figure 4.6 Multiple crack initiation sites at low (a) and higher (b) magnification and individual pits are shown in (c) and (d) in a specimen (A01N39) pre-corroded for 384 hours.

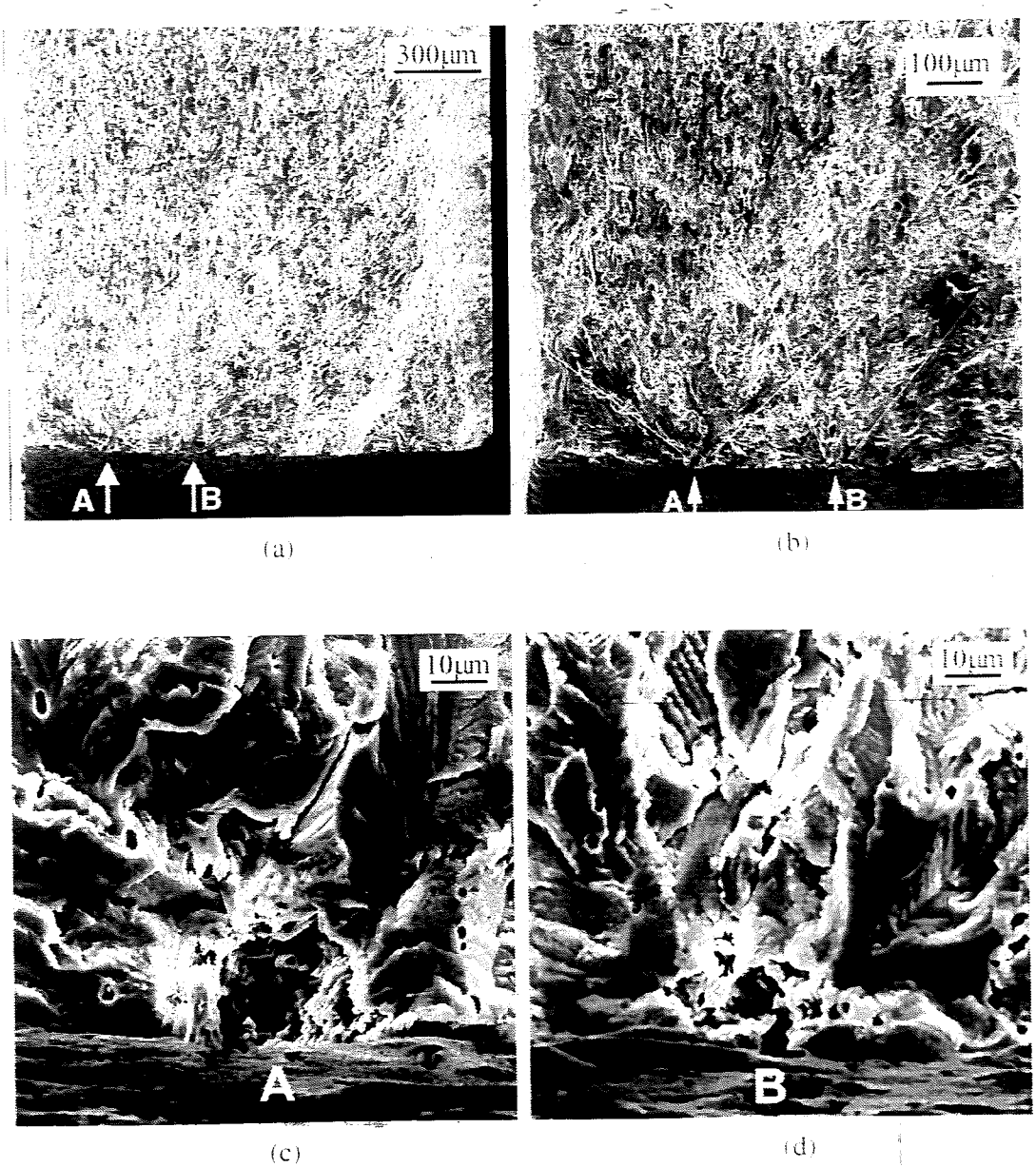

Figure 4.6 Multiple crack initiation sites at low (a) and higher (b) magnification and individual pits are shown in (c) and (d) in a specimen (A01N39) pre-corroded for 384 hours.

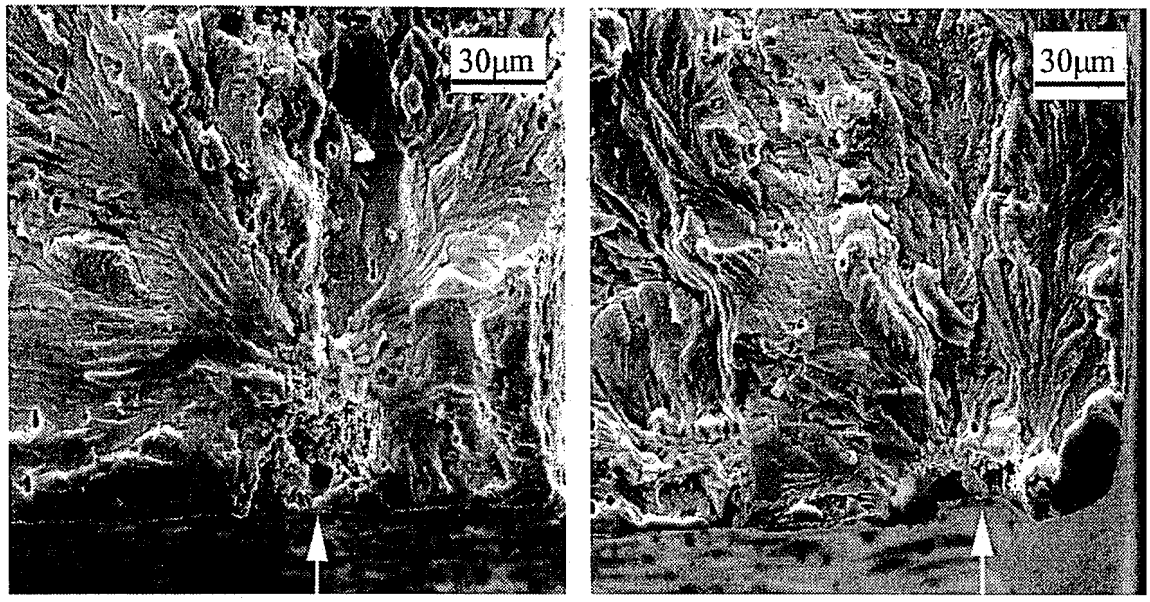

(a) (b)

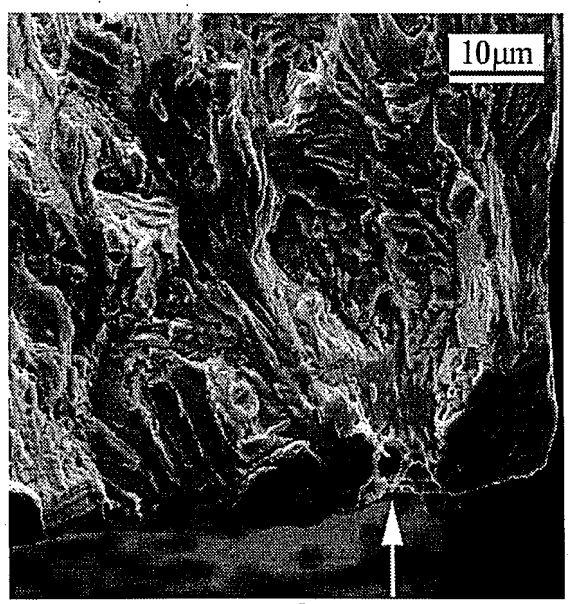

(c)

Figure 4.7 Initial pit sizes for (a) 384-hour pre-corrosion (A01N06), (b) 192-hour pre-corrosion (A01N34) and (c) 96-hour pre-corrosion (A01N07).

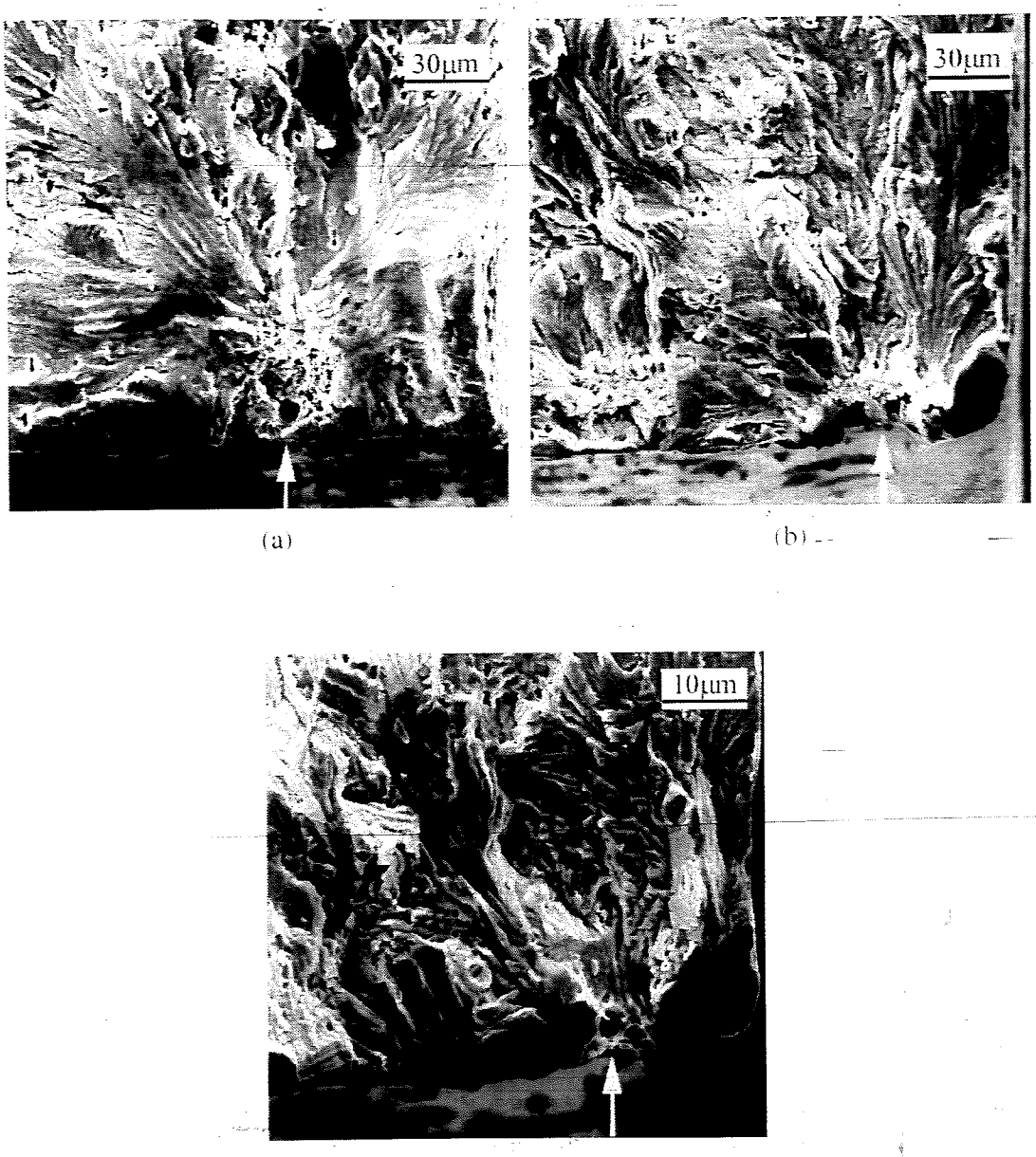

(a) (b)

(c)

Figure 4.7 Initial pit sizes for (a) 384-hour pre-corrosion (A01N06), (b) 192-hour pre-corrosion (A01N34) and (c) 96-hour pre-corrosion (A01N07).

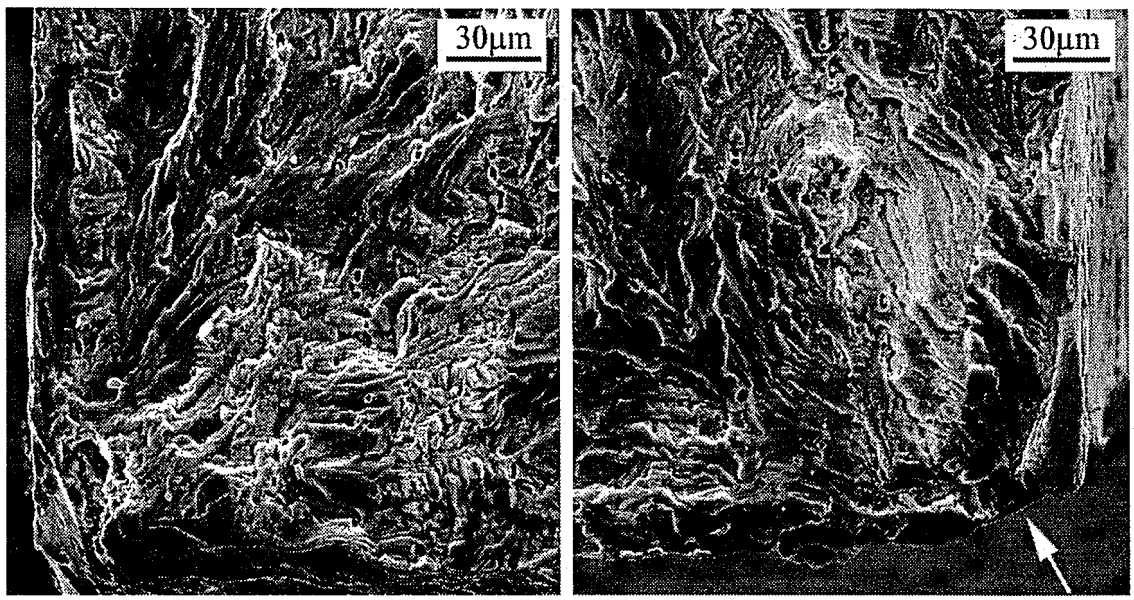

(a) (b)

Figure 4.8 Corner crack initiation sites for (a) a specimen (A01N21) pre-corroded for 384 hours and (b) a specimen (A01N14) pre-corroded for 192 hours.

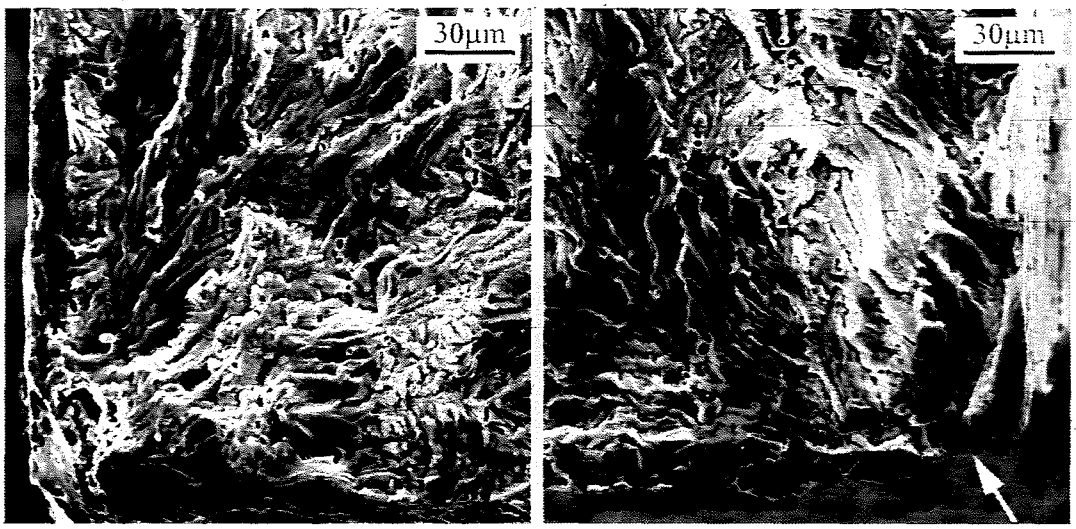

(a) (b)

Figure 4.8 Corner crack initiation sites for (a) a specimen (A01N21) pre-corroded for 384 hours and (b) a specimen (A01N14) pre-corroded for 192 hours.

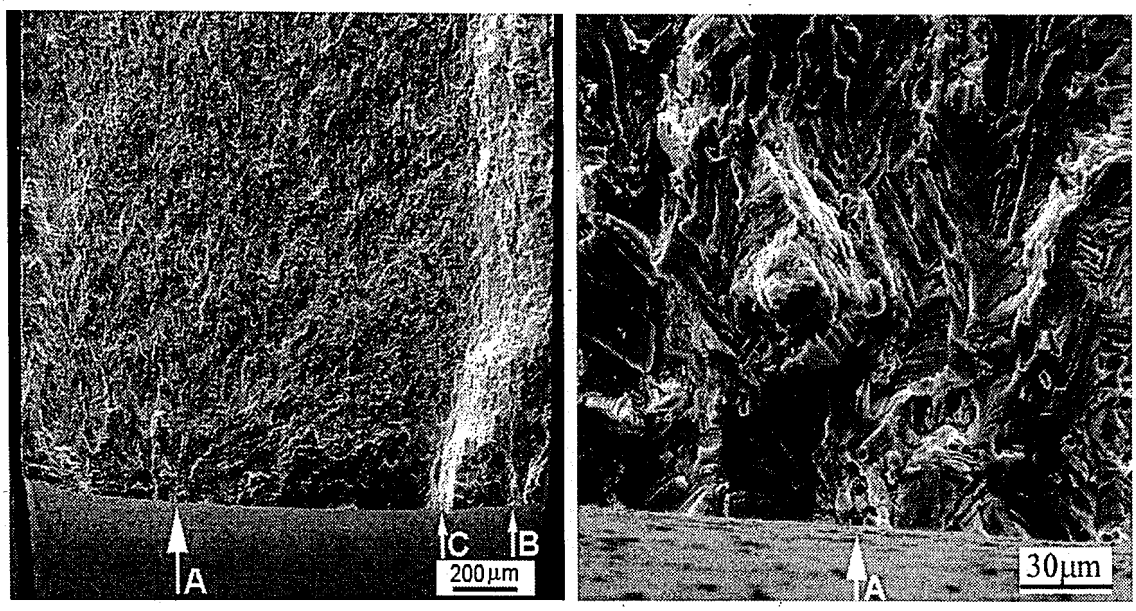

(a) (c)

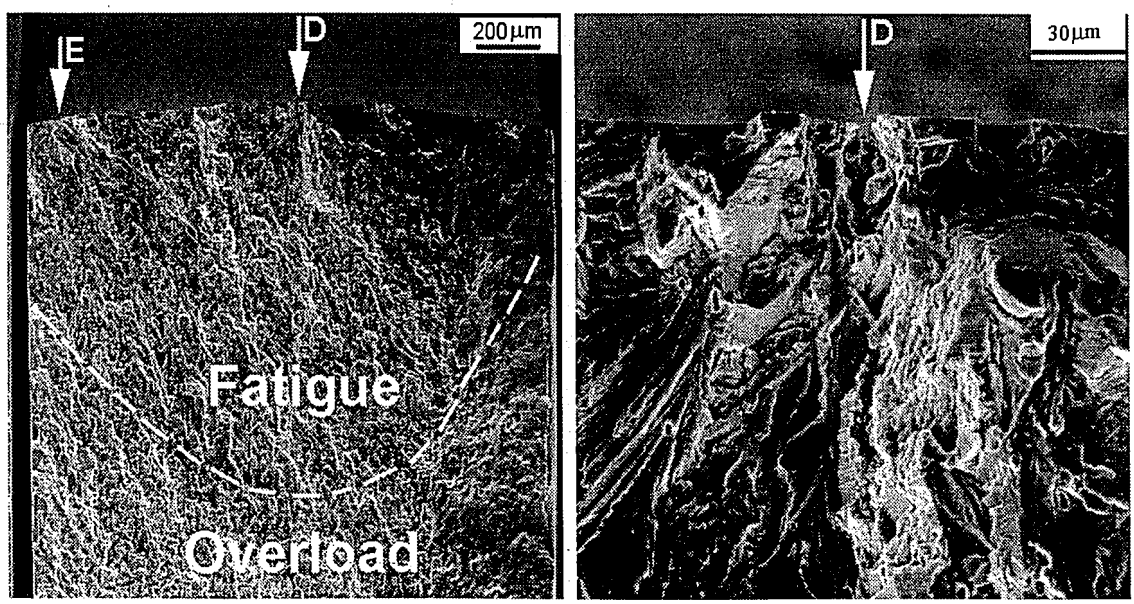

(b) (d)

Figure 4.9 Corrosion pits that nucleated dominant crack on both sides of the hole of a specimen (O13) pre-corroded for 24 hours.

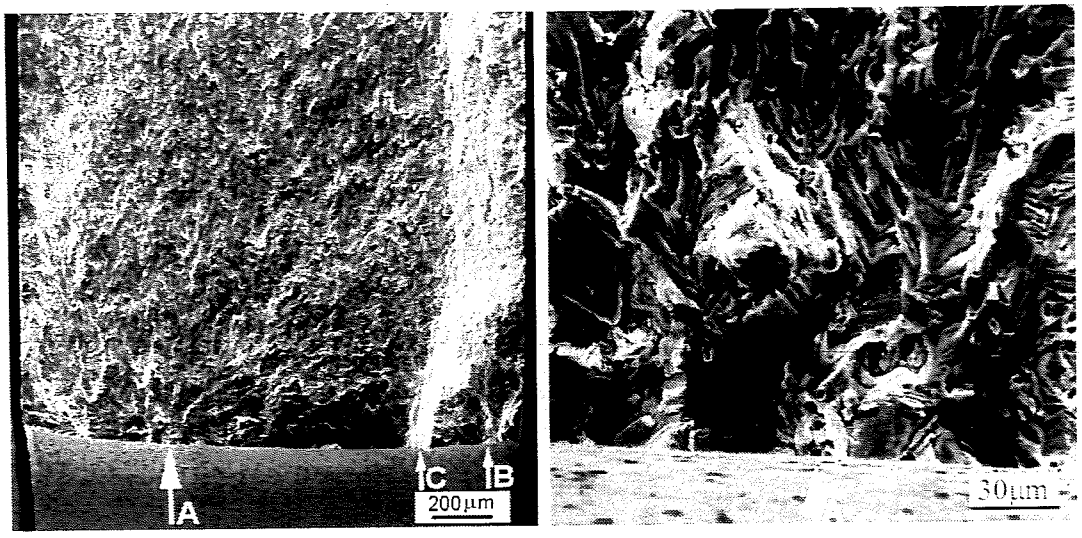

(a) (c)

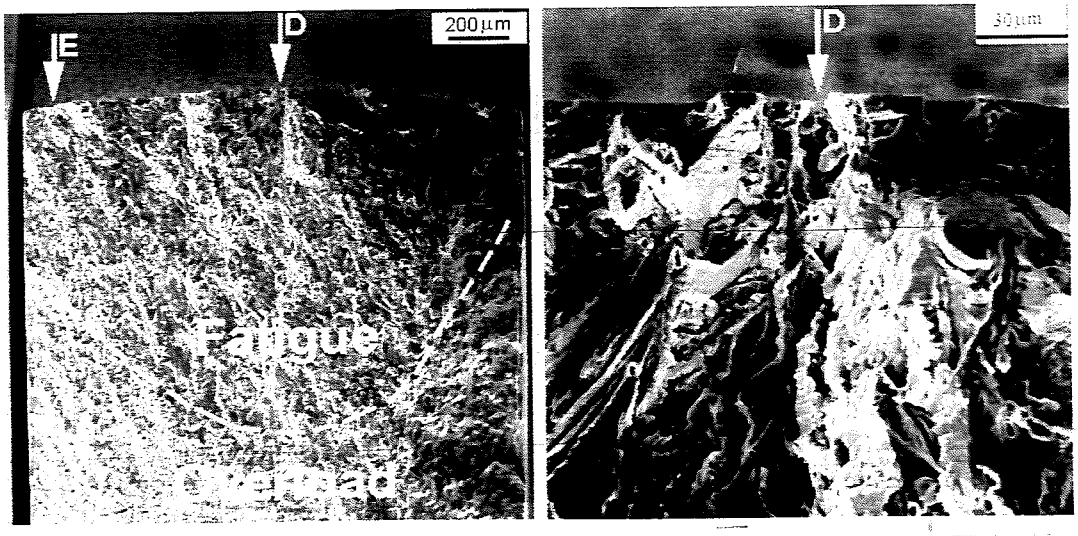

(b) (d)

Figure 4.9 Corrosion pits that nucleated dominant crack on both sides of the hole of a specimen (O13) pre-corroded for 24 hours.

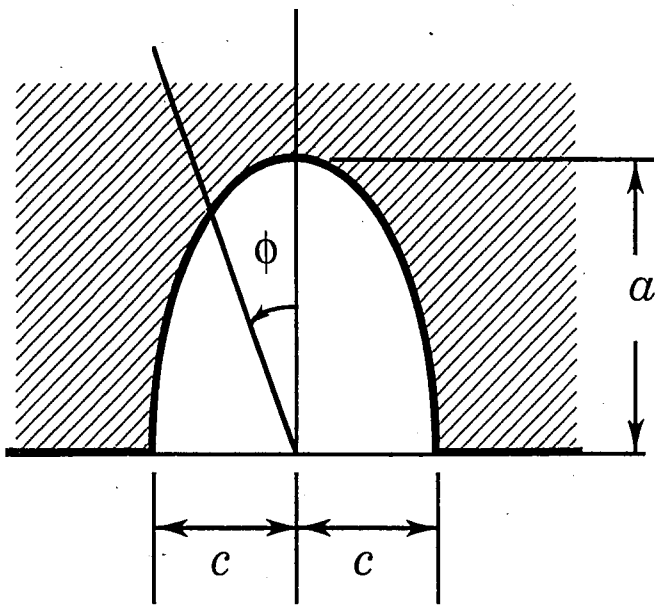

Figure 4.10 A schematic illustration of the equivalent semi-elliptic surface crack used as the initial crack geometry to model the FCG life [8].

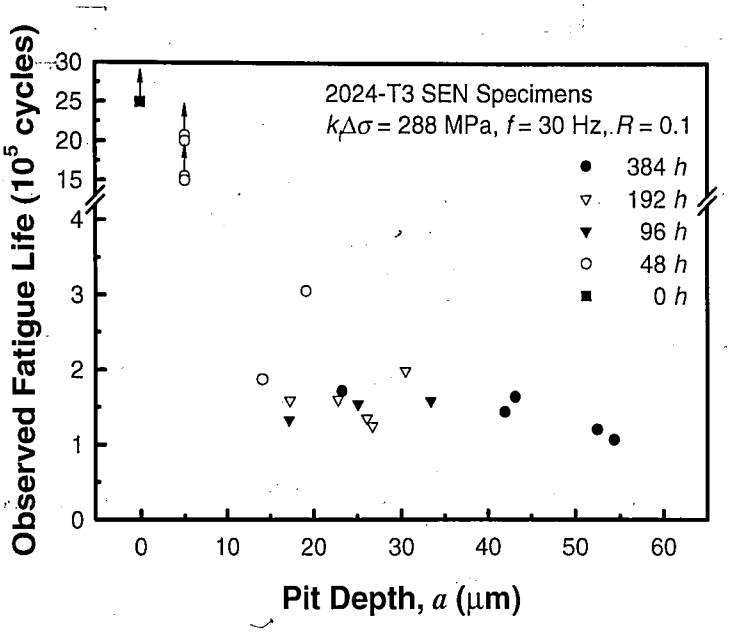

Figure 4.11 Reduction of fatigue life with increasing initial pit depth on SEN specimens.

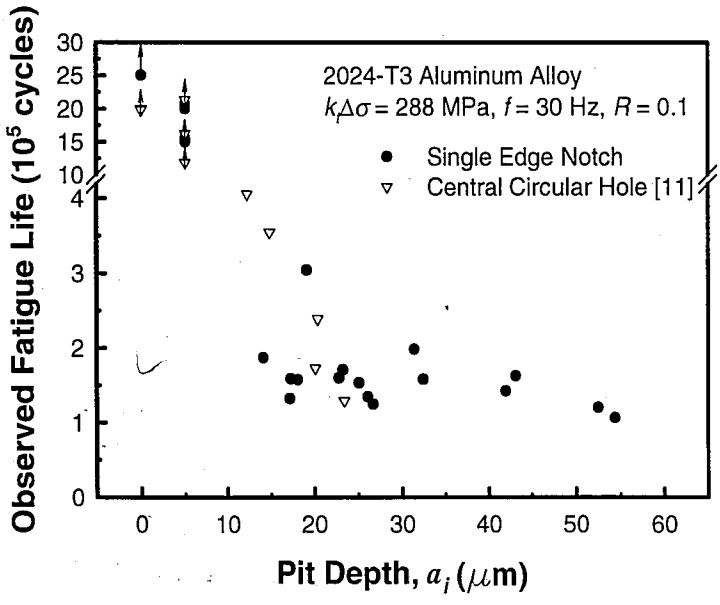

Figure 4.12 Reduction of fatigue life with increasing initial pit depth on SEN and CCH specimens.

CHAPTER 5 DISCUSSION

5.1 INTRODUCTION

The results showed the pre-corrosion can significantly reduce the subsequent fatigue lives of 2024-T3 aluminum alloy. The reduction resulted from the formation of corrosion pits that served as nuclei for fatigue cracking and effectively eliminated the early stage of fatigue crack growth (FCG). The results showed a strong correlation between fatigue lives and pit size *vis-à-vis* pre-corrosion time. It is appropriate to consider if fatigue lives could be estimated directly from information on pit sizes and FCG properties for the alloy. As a part of this consideration, previous results on 2024-T4 aluminum alloy tested in rotating bending by Harmsworth [10] included. Furthermore, the influence of variations in the size of dominant pits on the distribution of fatigue lives is considered.

5.2 2024-T4 ALUMINUM ALLOY [10]

For comparison with this study, previous results on the influence of pre-pitting time on the fatigue lives of a 2024-T4 alloy by Harmsworth [10] are reconsidered. In his study, rotating bending specimens were pre-pitted for 4 to 768 hours in an aqueous 20 (wt%) NaCl solution and were fatigue tested at a stress level of ±180 MPa at 3600 rpm in laboratory air.

The results are presented in Figure 5.1 as a function of pre-corrosion time, and show a similar trend in reduction of fatigue lives in the 2024-T3 aluminum alloy (*cf*, Figures 4.1 and 4.2). A similar trend in the reduction in fatigue lives with pit depth is

seen by comparing Figure 5.2 with Figures 4.11 and 4.12. Harmsworth suggested that secondary pits had little influence on fatigue life [10]. These results are in agreement with the current finding of the dominant influence of corrosion pits on fatigue life, and will be included in considering possible methodologies for life estimation

5.3 FATIGUE LIFE ESTIMATION

Based on recent studies, it was suggested that fatigue lives might be estimated from the initial pit size and the FCG properties using a linear fracture mechanics based crack growth analysis [33]. For simplisity, a power-law relationship for crack growth was used for fatigue life estimation;

$$\frac{da}{dN} = C_F(\Delta K)^{n_c};\ \left(\Delta K = \beta\,\Delta\sigma\sqrt{a}\right) \tag{5.1}$$

where C_F is crack growth rate coefficient, n_c is the power-law exponent, β is a geometric parameter that pertains to the crack, loading and component (specimen), ΔK is a stress intensity range, and a is a crack length. The material parameter, C_F, is a function of the test environment, as well as temperature and other factors as mentioned in chapter 2. For simple geometries and loadings, the relationship may be integrated directly. For more complex cases, a computer-aided numerical integration would be required.

5.3.1 2024-T4 ALUMINUM ALLOY [36]

For the simple, rotating bending case used by Dolley [36], fatigue lives of 2024-T4 aluminum alloy were estimated by direct integration from the power-law relationship. The specimen was a symmetrically tapered rotating bending so that no stress

concentration was considered, and the crack shape was assumed to have remained constant. By integration, a closed form solution is obtained;

$$N_f = \frac{2\left(\sqrt{\pi}\right)^{n_c}}{(n_c-2)C_F\left(\beta\cdot\Delta\sigma\right)^{n_c}}\left(\frac{1}{\sqrt{a_i}^{(n_c-2)}}-\frac{1}{\sqrt{a_f}^{(n_c-2)}}\right) \tag{5.2}$$

where, a_i is a initial crack size (pit depth), and a_f is a final crack size. The shape of initial corrosion pit was assumed to be hemispherical and to be equivalent to a semi-circular surface crack, the geometrical parameter, β, was assigned to $2.2\pi^{-1/2}$. The crack growth rate coefficient, C_F, is 1.3×10^{-11} (m cyc^{-1})(MPa$\sqrt{\text{m}}$)$^{-3.5}$ and power-law exponent, n_c, of 3.5 [33]. Because the final crack (a_f) is much greater than the initial crack (a_i), its contribution to life may be neglected. As such, the fatigue life depends simply on the initial crack size, or pit size, at a given applied stress.

The estimated fatigue lives were obtained by Dolley [36] and are compared to the observed fatigue lives in Table 5.1 and Figure 5.3. It was found that the majority of the data were within a scatter of factor 1.3, and the largest differences were approximately a factor of 2. The difference may be attributed to three sources. Experimentally, the accuracy of pit depth measurement was limited by the available optical technique at the time. Also, the aspect ratio of the pits were not and their determined influence on fatigue life was not reflected in the data presentation. Analytically, a constant aspect ratio was assumed such that its influence is not incorporated. Given these uncertainties, the agreement is deemed to be good. The agreement suggests that fatigue lives can be estimated directly from the nucleating pit size and the crack growth characteristics, and

that crack nucleation from a corrosion pit is rapid and its contribution to fatigue life may be neglected.

5.3.2 2024-T3 ALUMINUM ALLOY

Because notched specimens were used in this study for the 2024-T3 aluminum alloy, a numerical integration procedure was required to account for the stress concentration of the notch or hole, its influence on the stress intensity factor, and the transition from a surface or corner crack to a through-thickness crack as it grows away from the notch or hole surface. Thus, a crack growth analysis life prediction program, AFGROW, was used [34]. AFGROW permits cycle-by-cycle integration and tracks changes in crack shape as it grows.

To begin the calculation, specifications of material, and specimen and crack geometry were made, and extrinsic parameters like dimensions, loading, and load ratio were entered. FCG properties were specified by the power-law relationship given in Eq. (5.1) by using C_F of 3.95×10^{-11} (m cyc^{-1})(MPa$\sqrt{\text{m}}$)$^{-3.55}$ and n_c of 3.55 [33]. By assuming the initial crack to be semi-circular in shape, the fatigue life was estimated from the initial pit sizes out to the end of the flat (tensile) mode or the crack length at the onset of fast fracture; both of which were verified by the fractography.

The estimated lives for the 2024-T3 SEN and CCH specimens are listed in Table 5.2 and in Table 5.3, respectively, in comparison to the observed lives. The comparison is also shown in Figure 5.4. Uncertainty in estimated life associated with ±10% error in pit depth measurement was computed and indicated by the "*error*" bars on each point.

Similar to the 2024-T4 alloy (Figure 5.3), the estimated fatigue lives for 2024-T3 alloy were in good agreement with the observed fatigue life with a similar degree of scatter. The reasons for the scatter were essentially the same, except that the technique for pit size measurement is much more accurate here. It should be noted that the fatigue lives of specimens with corner cracks were systematically underestimated. This is discrepancy is most likely related to the numerical integration routine. Based on the results, it is clear that fatigue lives of pre-corroded specimens can be accurately estimated through using the FCG properties, initial pit sizes, and applied load.

5.4 Probabilistic Analysis

To determine if the distribution in fatigue lives at a given pre-corrosion time is related to the distribution in pit sizes, an analysis was performed on the five 2024-T3 SEN specimens precorroded for 384 hours. All of the corrosion pits on the fracture surfaces, either as surface or corner cracks, were examined and recorded. A cumulative distribution function (*cdf*) of probability of occurrence (PoO) of pit of a given depth was fitted to the data as shown in Figure 5.5 [15,39]. The PoO is the probability of finding a pit depth that exceeds a specified pit depth, *a*. Weibull probability paper was used for convenience [40]. The numbers given 1 to 5 represented the distribution of dominant pit depths for each of the five specimens in ascending order.

Based on the PoO, 100 pit depths were generated by the Monte Carlo method, and were used as initial crack sizes for determining the distribution in fatigue lives using AFGROW. To examine the influence of the aspect ratio of the corrosion pits, c/a = 0.6 and c/a = 1.0 were used. A final crack length of 4 mm was used; however, because of the

relatively small size of the initial pit, the estimated lives are not sensitively affected by this choice. The estimated distributions are shown in Figure 5.6, along with the experimental data (as solid circles) for the 384-hour pre-corroded specimens.

The comparison shows that the distribution in fatigue lives is well described in terms of the distribution in the initial pit sizes. In Figure 5.6, the order of pits #2 and #3 in actual fatigue lives is reversed relative to their ranking in pit depth (see Figure 5.5). This reverse is attributed to the influence of aspect ratio. Specifically, pit #2 was deeper, but with a lower aspect ratio than the shallower pit #3. As such, a larger number of fatigue cycles would be required to produce fatigue failure. This explanation is consistent with the predicted response as seen through a comparison between the distribution curves at any given value of *cdf*.

Table 5.1 Comparison of the observed fatigue life [10] and the estimated fatigue life [36].

Corrosion Time (hours)	Pit depth (μm)	Observed Fatigue life (cycles)	Estimated Fatigue Life (cycles)
4	10.16	2,744,900	3,465,987
4	17.78	2,117,400	2,277,972
4	7.62	1,938,200	4,300,620
4	35.56	1,101,900	1,354,490
4	38.10	1,100,000	1,286,185
8	30.48	1,766,100	1,520,499
8	35.56	1,608,200	1,354,490
8	68.58	896,300	827,655
8	33.02	781,400	1,431,906
8	71.12	426,100	805,385
24	50.80	1,006,600	1,036,572
24	91.44	780,100	667,030
24	55.88	717,500	965,061
24	78.74	674,500	746,192
24	104.14	613,300	605,040
48	53.34	2,247,200	999,327
48	88.90	907,400	681,273
48	86.36	703,800	696,246
48	129.54	611,100	513,682
48	104.14	407,200	605,040
96	111.76	776,300	573,829
96	101.60	498,100	616,349
96	104.14	491,900	605,040
96	104.14	491,100	605,040
96	121.92	301,800	537,577
192	154.94	690,000	449,133
192	109.22	659,000	583,809
192	142.24	613,700	478,885
192	109.22	580,700	583,809
192	132.08	471,400	506,255
384	134.62	555,300	499,074
384	144.78	542,500	472,570
384	142.24	390,300	478,885
384	190.50	376,300	384,659
384	236.22	286,100	327,348
768	187.96	531,300	388,551
768	198.12	505,700	373,509
768	172.72	448,000	413,990
768	238.76	444,500	324,733
768	294.64	320,300	277,350

Table 5.2 Results of estimated fatigue life in ±10% pit size error on 2024-T3 SEN specimens using AFGROW.

Specimen Number	Corrosion Time (hours)	Observed Fatigue Life (cycles)	Estimated Fatigue Life (cycles)		
			Upper Bound	Lower Bound	Base
A01N17	48	304,594	297,700	257,700	276,000
A01N18	48	187,144	317,300	274,600	294,100
A01N07	96	153,691	173,500	150,400	160,800
A01N15	96	132,808	238,500	207,300	221,600
A01N36	96	158,056	130,800	113,100	121,100
A01N12	192	159,106	172,500	149,600	160,000
A01N14	192	160,121	140,300	121,400	130,000
A01N19	192	198,381	185,000	161,200	172,000
A01N23	192	134,965	155,700	136,200	145,500
A01N34	192	125,216	152,500	132,500	141,700
A01N06	384	106,318	120,200	104,200	111,500
A01N21	384	162,567	126,200	109,100	116,900
A01N30	384	142,584	104,100	88,700	97,300
A01N32	384	120,168	106,000	93,600	99,200
A01N39	384	171,078	176,100	153,300	163,700

Table 5.3 Results of estimated fatigue life in ±10% pit size error on 2024-T3 CCH specimens using AFGROW.

Specimen Number	Corrosion Time (hours)	Observed Fatigue Life (cycles)	Estimated Fatigue Life (cycles)		
			Upper Bound	Lower Bound	Base
O8	24	239,202	277,800	242,200	258,100
O13	24	173,306	207,700	180,700	193,100
C1	100	129,556	201,800	175,200	187,300
C8	100	405,784	287,400	280,700	283,300
C9	100	354,830	372,300	321,800	344,700

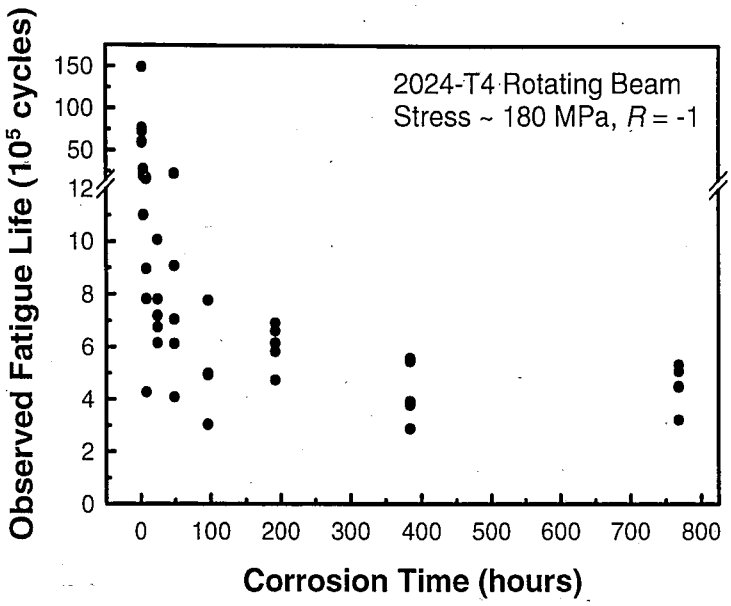

Figure 5.1 Reduction of fatigue life for 2024-T4 rotating beam specimens as a function of corrosion time [10].

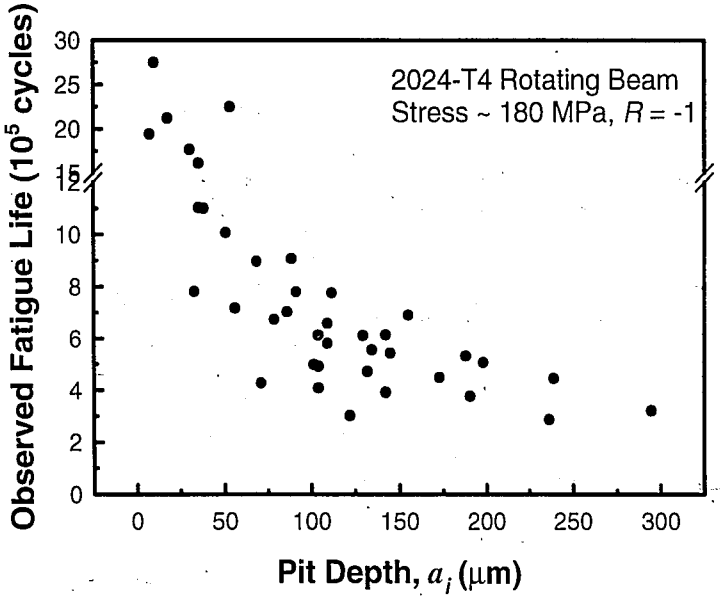

Figure 5.2 Reduction of fatigue life for 2024-T4 rotating beam specimens as a function of pit depth [10].

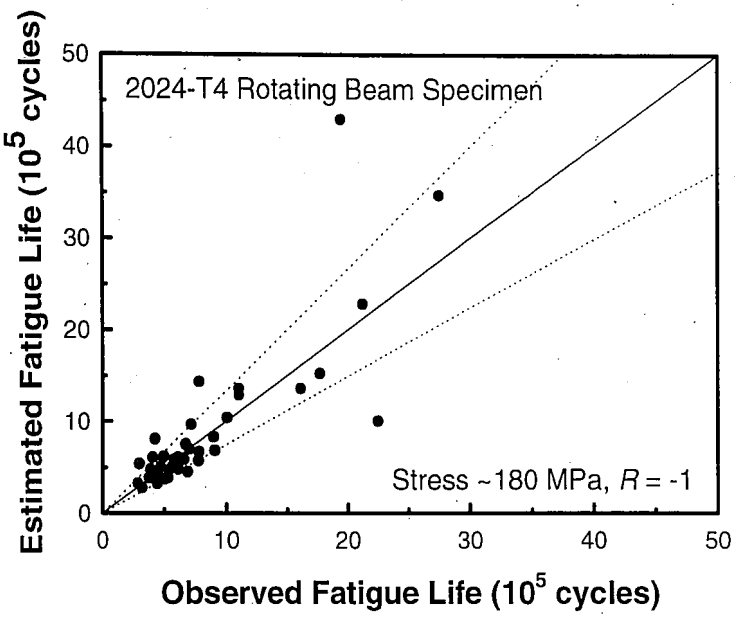

Figure 5.3 Comparison of the observed vs. estimated fatigue life for 2024-T4 alloy [36].

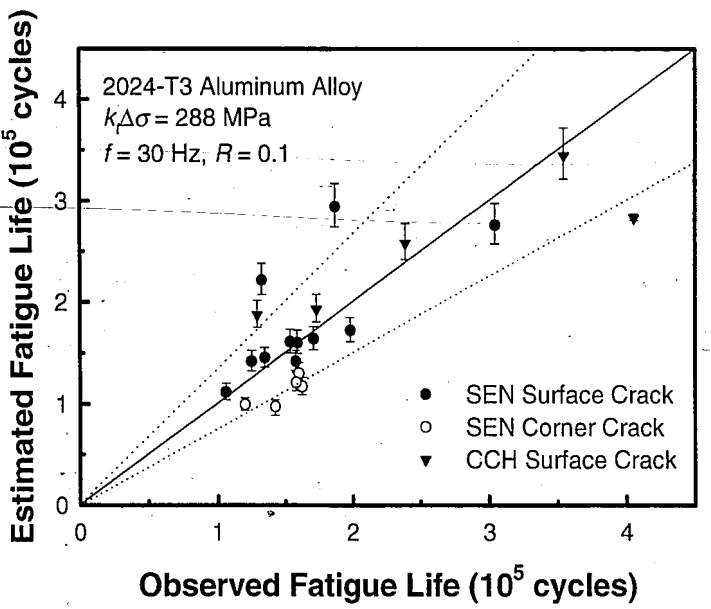

Figure 5.4 Comparison of the observed vs. estimated fatigue life for 2024-T3 alloy.

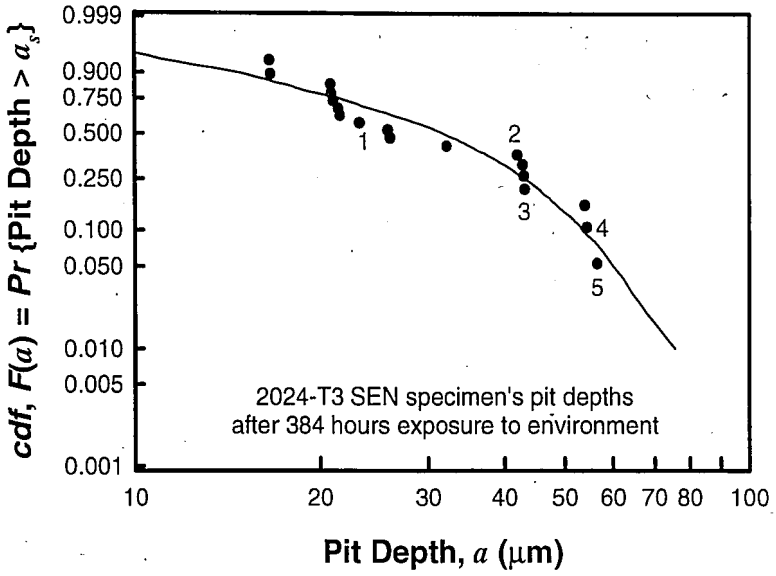

Figure 5.5 Pit depth distribution following 384 hours pre-corrosion (a) actual pit sizes (data points) and (b) estimated pit depth model (line) [15,39].

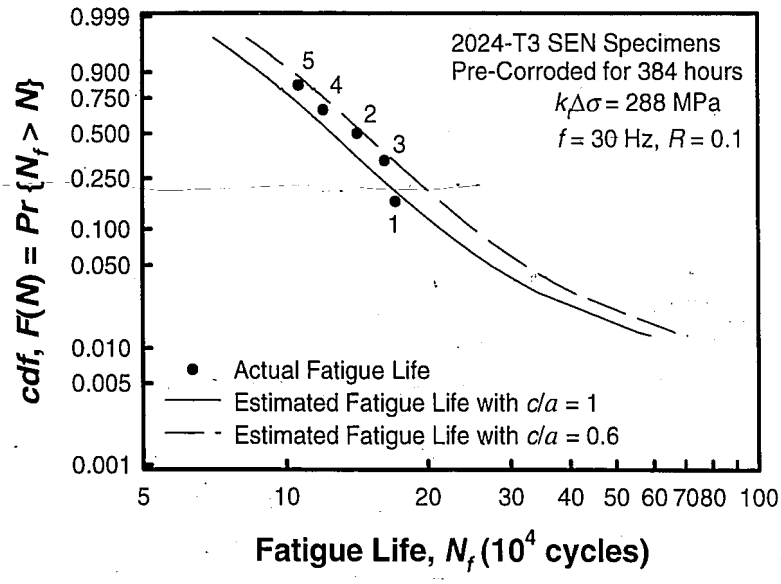

Figure 5.6 Estimated and actual distributions of fatigue life showing that the distribution of pit depth dictates the distribution of fatigue life.

CHAPTER 6 SUMMARY AND FUTURE WORK

6.1 SUMMARY AND CONCLUSION

An experimental study was conducted to characterize the influence of pre-existing corrosion pits on fatigue life. The approach began by assessing if the corrosion pits as nuclei affected the fatigue life. Based on the finding, an assessment was made to determine and if the fatigue life can be estimated from the initial pit size and the FCG properties so that an engineering framework can be established for life prediction and probabilistic analysis.

Pitting-induced fatigue testing was performed on a 2024-T3 aluminum alloy in air at room temperature. A stress of 288 MPa, frequency of 30 Hz and load ratio of 0.1, was applied to the specimens' notch that were pre-corroded from 48 to 384 hours (2 to 16 days) in 0.5M NaCl solution at room temperature. Post-fracture examinations of the fracture surfaces were made to identify the crack nucleation sites and the sizes of the corrosion pits.

Fatigue life of the 2024-T3 aluminum alloys was reduced significantly due to the presence of pitting corrosion. Corrosion pits acted as pre-existing flaws in the material nucleating fatigue cracks. The reduction in fatigue life depended upon the pre-corrosion time and in turn the initial pit size. As longer pre-corrosion time led to deeper initial pits, the fatigue life was reduced significantly compared to the fatigue life of the un-corroded material. Post-fracture fractography revealed that all of the fatigue cracks initiated at corrosion pits. Fatigue life was estimated using a fracture mechanics approach and was

in good agreement with the actual fatigue life. This showed that the total fatigue life could be estimated if the initial crack size, local stress, and FCG properties were known.

A probabilistic analysis showed that the distribution in fatigue lives was directly related to the distribution in the size of crack nuclei, but is also expected to reflect variations in crack growth properties. This finding provides a direct connection between the conventional and fracture mechanics based approaches to corrosion fatigue in that it suggests that the S-N response might be directly predicted from linear fracture mechanics considerations of crack growth.

6.2 Future Work

While the work done for this research has contributed to a greater understanding of the mechanisms for fatigue cracking subjected to pre-corrosion, more work remains to be done. A mechanically based probabilistic analysis supported that increasing the pre-corrosion time by considering deeper pit depth decreases the fatigue life significantly. The dominant corrosion pit in low pre-corrosion time controls the entire fatigue life from the fatigue life estimation. In highly corroded samples, the influence of multiple crack initiation sites needs to be better understood to develop a more complete model of the underlying process for fatigue life estimation.

Many studies have been performed to improve the understanding of the kinetics and mechanisms of environmentally affected fatigue cracking of structural materials. This study has made use of simple sinusoidal loading with constant amplitude and frequency. This work need to be extended to better represent the loading conditions in

service. This extension would allow for a more complete characterization of the material response and the validation of the life estimation.

REFERENCES

1. United States Congress House Committee on Science, Space, and Technology, (1988), 'Research and Development on Fatigue and Corrosion in Aging Aircraft', *Report (Report / 100th Congress, 2nd session, House of Representatives; 100-895)*, Washington, D.C., U.S. G.P.O., pp.1-5.

2. Chang, C. I. and Sun, C. T., (1995), 'Aging Aircraft Science and Technology Issues and Challenge and USAF Aging Aircraft Problem', *Structural Integrity in Aging Aircraft*, Chang, C. I. And Sun, C. T., eds., ASME International, Mechanical Engineering Congress and Exposition, AD-Vol.47, pp.1-7.

3. Wei, R. P. and Speidel, M. O., (1971), 'Phenomenological Aspects of Corrosion Fatigue', *Corrosion Fatigue; Chemistry, Mechanics and Microstructure*, NACE-2, eds., Devereux, O., McEvily, A. J., and Staehle, R. W., National Association of Corrosion Engineers, Houston, Texas 77027, pp.379-380.

4. Burynski, R. M., Chen, G-S., and Wei, R. P., (1995), 'Evolution of Pitting Corrosion in a 2024-T3 Aluminum Alloy', *Structural Integrity in Aging Aircraft*, Chang, C. I. and Sun, C. T., eds., ASME International, Mechanical Engineering Congress and Exposition, AD-Vol.47, pp.175-183.

5. Burynski, R. B., (1994), 'Corrosion Response of a 2024-T3 Alloy in 0.5M NaCl Solution', MS Thesis, Lehigh University, Bethlehem, PA.

6. Cawley, N. R., (1995), 'Models for the Spatial Statistics of Constituent Particles and Corrosion Pits', Ph.D Dissertation, Lehigh University, Bethlehem, PA.

7. Chen, G-S., Gao, M., and Wei, R. P., (1996), 'Microconstituent-Induced Pitting Corrosion in Aluminum Alloy 2024-T3', *Corrosion Science*, Vol.52 No.1, pp.8-15.

8. Chen, G-S., Wan, K-C., Gao, M., and Wei, R. P., (1996), 'Transition from Pitting to Fatigue Crack Growth-Modeling of Corrosion Fatigue Crack Nucleation in a 2024-T3 Aluminum Alloy', *Materials Science and Engineering*, Vol.219, pp.126-132.

9. Liao, C. M., (1998), 'Particle Induced Pitting Corrosion of Aluminum Alloys', Ph.D Dissertation, Lehigh University, PA, pp.24-28.

10. Harmsworth, C. L., (1961), 'Effect of Corrosion on the Fatigue Behavior of 2024-T4 Aluminum Alloy', *ASD TR 61-121*, Aeronautical Systems Division, Wright-Patterson AFB, Ohio.

11. DeMoyer, J., (1996), Unpublished result, Lehigh University.

12. Chen, G-S., Gao, M., Harlow, D. G., and Wei, R. P., (1994), FAA/NASA International Symposium on Advanced Structural Integrity Methods for Airframe Durability and Damage Tolerance, *NASA Conference Publication*, 3274, Langley Research Center, Hampton, VA 23681, pp.157-173.

13. Chen, G-S., Liao, C. M., Wan, K-C., Gao, M., and Wei, R. P., (1997), 'Pitting Corrosion and Fatigue Crack Nucleation Effects of the Environment on the Initiation of Crack Growth', *ASTM STP 1298*, eds., Van Der Sluys, W. A., Piascik, R. S., and Zawierucha, R., (Philadelphia, PA: American Society for Testing and Materials), pp.18-33.

14. Piascik, R. S. and Willard, S. A., (1994), 'Effect of Corrosion on the Fatigue Behavior of 2024-T3 Aluminum Alloy', *Fatigue of Engineering Materials & Structures*, Vol.17, pp.1247-1259.

15. Harlow, D. G. and Wei, R. P., (1994), 'Probability Approach for Prediction of Corrosion and Corrosion Fatigue Life', *American Institute of Aeronautics and Astronautics*, Vol.32, pp.2072-2079.

16. Haigh, B. P., (1917), 'Experiments on the Fatigue of Brasses', *Journal of the Institute of Metals*, Vol.18, pp.55-86.

17. Moore, R. R., (1927), 'Effect of Corrosion Upon the Fatigue Resistance of Thin Duralumin', *ASTM Tentative Standards*, Vol.27, No.11, pp.128-133.

18. Gough, H. J. and Sopwith, D. G., (1932), 'Atmospheric Action as a Factor in Fatigue of Metals', *Journal of the Institute of Metals*, Vol.49, pp.93-122.

19. Paris, P. and Erdogan, F., (1963), 'A Critical Analysis of Crack Propagation Laws', *Journal of Basic Engineering, Transactions of the ASME*, Vol.85, pp.528-534.

20. Wei, R. P., (1970), 'Some Aspects of Environment-Enhanced Fatigue-Crack Growth', *Engineering Fracture Mechanics*, Vol.1, pp.633-651.

21. El-Soudani, S. M. and Pelloux, R. M., (1973), 'Influence of Inclusion Content on Fatigue Crack Propagation in Aluminum Alloys', *Metallurgical Transactions*, Vol.4, pp.519-531.

22. Wei, R. P., (1978), 'Fracture Mechanics Approach to Fatigue Analysis in Design', *Journal of Engineering Materials and Technology*, Vol.100, pp.113-120.

23. Ritchie, R. O., (1978), 'Environment-Sensitive Fracture of Engineering Materials', Foroulis, Z. A.; eds., TMS-AIME, pp.538-564.

24. Wei, R. P., Pao, P. S., Hart, R. G., Weir, T. W., and Simmons, G. W., (1980), 'Fracture Mechanics and Surface Chemistry Studies of Fatigue Crack Growth in an Aluminum Alloy', *Metallurgical Transactions A*, Vol.11A, pp.151-158.

25. Vasudévan, A. K. and Suresh, S., (1982), 'Influence of Corrosion Deposits on Near-Threshold Fatigue Crack Growth Behavior in 2XXX and 7XXX Series Aluminum Alloys', *Metallurgical Transactions A*, Vol.13A, pp.2271-2280.

26. Ricker, R. E. and Duquette, D. J., (1988), 'The Role of Hydrogen in Corrosion Fatigue of High Purity Al-Zn-Mg Exposed to Water Vapor', *Metallurgical Transactions A*, Vol.19A, pp.1775-1783.

27. Gdoutos, E. E., (1984), *Problems of Mixed Mode Crack Propagation*, Martinus Nijhof Publishers, Chapter 1-2, pp.1-39.

28. Hoeppner, D. W., (1979), 'Model for Prediction of Fatigue Lives Based upon a Pitting Corrosion Fatigue Process', *Fatigue Mechanisms*, STP 675, Fong, T. J., eds., ASTM, Philadelphia, PA, p.841.

29. Muller, M., (1982), 'Theoretical Considerations on Corrosion Fatigue Crack Initiation', *Metallurgical Transactions*, Vol.13A, p.649.

30. Kondo, Y., (1989), 'Prediction of Fatigue Crack Initiation Life Based on Pit Growth', *Corrosion*, Vol.45, No.1, pp.7-11.

31. Kondo, Y. and Wei, R. P., (1989), 'Approach on Quantitative Evaluation of Corrosion Fatigue Crack Initiation Condition', *Proceedings EVALMAT*, pp.135-142.

32. Wei, R. P. and Harlow, D. G., (1996), 'Corrosion and Corrosion Fatigue of Airframe Materials', *DOT/FAA/AR-95/76*, The National Technical Information Service, Springfield, Virginia 22161.

33. Wei, R. P., (1997), 'Corrosion Fatigue: Science and Engineering', *Recent Advances in Corrosion Fatigue*, Sheffield, UK.

34. Crack Growth Life Prediction Program, AFGROW (1994), http://fibec.flight.wpafb.af.mil/fibec/afgrow.html.

35. Chaudhuri, J., Tan, Y. M., Patni, K., and Eftekhari, A., (1992), 'Comparison of Corrosion-Fatigue Properties of 6013 Bare, Alclad 2024, and 2024 Bare Aluminum Alloy Sheet Materials', *Journal of Materials Engineering and Performance*, Vol.1, pp.91-96.

36. Dolley, E. J., (1997) Unpublished result, Lehigh University.

37. *Metals Handbook*, (1982), 9th Ed., Vol.5, Surface Cleaning, Finishing and Coating, ASM International (Metals Park, Ohio), p.578.

38. Wan, K-C., (1996), 'Mechanical and Chemical Aspects of Corrosion Fatigue of a 2024-T3 Aluminum Alloy in the Short Crack Regime', Ph.D Dissertation, Lehigh University, Bethlehem, PA.

39. Harlow, D. G. and Wei, R. P., (1998), 'Probability Aspects of Aging of Airframe Materials: Damage versus Detection', *The Third Pacific Rim International Conference on Advanced Materials and Processing (PRICM 3)*, Edited by Imam, M. A., DeNale, R., Hanada, S., Zhong, Z., and Lee, D. N., eds., The Minerals, Metals & Material Society, pp.2657-2666.

40. Nelson, L. S., (1967), 'Weibull Probability Paper', *Industrial Quality Control*, General Electric Lamp Division, Cleveland, Ohio, p.452.

VITA

Baekho Lee was born January 25, 1968 in Seoul, Korea to Boonim and Dukmoon Lee. He earned his Bachelor of Science in Metallurgy and Materials Science from Hanyang University, Korea in February 1994. While at Hanyang, he received a Scholarship for academic excellence in 1992. During his study, he joined the Army in May 1989 for 2 years serving his duty in army aviation intermediate unit as certified helicopter repairman, and was awarded for the best of conduct recognition three times.

After graduation, he became a tutor of mathematics in private institutes for middle and high school students until he came to U.S. for graduate study. For the last year of teaching, he was also employed by Kumhwa Precision Eng. as CAD designer.

In June 1996, he began his graduate work at Lehigh University in Bethlehem, Pennsylvania. At Lehigh, he worked under the guidance of Dr. Robert P. Wei in an effort to earn a Master of Science in Mechanical Engineering. His thesis research involved the influence of pre-existing corrosion pits on fatigue life of a 2024-T3 aluminum alloy. Part of the results of this thesis research was presented at the 1998 TMS fall meeting under the same title. As co-author a technical paper is being prepared and will be submitted to the journal of *Fatigue and Fracture of Engineering Materials and Structures.*

Baekho is a member of joint American Society of Metals (ASM International) and The Minerals, Metals & Materials Society.

Mr.Lee married Wonhee Kim in May 1996, and they have their first baby, Jenny, born in August 1997.

END

OF

TITLE